Growth and decay of discrete nonlinear Schrödinger breathers interacting with internal modes or standing-wave phonons

Magnus Johansson and Serge Aubry
Laboratoire Léon Brillouin (CEA-CNRS), CEA Saclay,
F-91191 Gif-sur-Yvette Cedex, France

We investigate the long-time evolution of weakly perturbed single-site breathers (localized stationary states) in the discrete nonlinear Schrödinger (DNLS) equation. The perturbations we consider correspond to time-periodic solutions of the linearized equations around the breather, and can be either (i) spatially localized, or (ii) spatially extended. For case (i), which corresponds to the excitation of an internal mode of the breather, we find that the nonlinear interaction between the breather and its internal mode always leads to a slow growth of the breather amplitude and frequency. In case (ii), corresponding to interaction between the breather and a standing-wave phonon, the breather will grow provided that the wave vector of the phonon is such that the generation of radiating higher-harmonics at the breather is possible. In other cases, breather decay is observed. This condition yields a limit value for the breather frequency above which no further growth is possible. We also discuss another mechanism for breather growth and destruction which becomes important when the amplitude of the perturbation is non-negligible, and which originates from the oscillatory instabilities of the nonlinear standing-wave phonons.

I. INTRODUCTION

The concept of nonlinear self-localization is of importance for many physical phenomena, and has appeared in a number of different contexts since the pioneering work by Landau [1] on the polaron problem in the 1930s. In recent years, much attention has been devoted to studies of spatially localized and time-periodic vibrational modes in anharmonic lattices (see e.g. [2], [3] for recent reviews). The general existence of such modes, which have been termed *discrete breathers*, or *intrinsic localized modes*, as robust solutions to nonlinear (and in general non-integrable) lattice-equations was suggested in 1988 by Takeno *et al* [4]. Later, their existence was rigorously proven under rather general conditions by MacKay and Aubry [5] by considering the limit of uncoupled oscillators (the so called *anticontinuous* or *anti-integrable* limit). By means of the implicit function theorem, they showed that the trivial solution of a single-site localized vibration at the uncoupled limit could be continued into a localized breather solution for non-zero coupling between the oscillators, provided that the individual oscillators are anharmonic, and that no multiples of the breather frequency resonate with the bands of linear excitations (phonons). As was demonstrated first in [6], the ideas of the rigorous proof can be turned into an efficient numerical scheme to calculate breather solutions to any desired accuracy. Since the discrete breathers appear under very general conditions in anharmonic lattices and provide efficient means of energy localization, they have been proposed as candidates to explain experimentally observed localization of energy in many different physical areas, e.g. DNA dynamics [7].

Although, from a fundamental and mathematical viewpoint, the existence theorems for discrete breathers provide an important cornerstone for understanding the dynamics of anharmonic lattices, it is probably of even larger physical importance to understand the behaviour of a system close to an exact breather solution. By linearizing the lattice-equations around the exact solution, one can obtain an approximate description of the dynamics of weakly perturbed breathers, and in particular the linear stability properties determining whether small perturbations will grow exponentially or not. It was shown in [2], [5] that the simplest, single-site, breathers are generally linearly stable close to the uncoupled limit, and numerical investigations using standard Floquet analysis (see e.g. [8]) have shown that linearly stable breathers typically exist also for rather large values of the inter-site coupling. However, when considering time-scales large compared to the breather period, the mere linear stability of a breather does no longer guarantee the eternal existence of the breather in the presence of small perturbations, and there are still many questions remaining concerning the different mechanisms by which breathers may grow or decay, or possibly finally be destroyed. If the breathers have a finite life-time, the determination of this life-time is of large importance for understanding the role of breathers in real systems.

It is the purpose of this paper to investigate in more detail some mechanisms for breather growth and decay in a simple model system, the discrete nonlinear Schrödinger (DNLS) equation. The DNLS equation is generic in the sense that it describes slowly (in time) varying modulational waves in discrete systems in a 'rotating-wave' approximation (see e.g. [9,10]); however, due to its extra symmetry properties (see Sec. II) it exhibits some nongeneric features among discrete systems, e.g. exact quasiperiodic breathers [11]. The single-site breathers of the DNLS equation are stationary states which are linearly stable for all inter-site coupling, and which reduce to the NLS soliton in the

continuum limit (see e.g. [5,11–15]). An important application appears in nonlinear optics, where the single-site DNLS-breather describes a discrete spatial soliton in an array of weakly coupled waveguides [16,17]; recent experimental observations [18] confirm the successful use of the DNLS-model in this context.

Some recent numerical investigations [19] have shown that DNLS-breathers can be spontaneously created from noisy backgrounds, in a similar manner as was previously observed for Klein-Gordon [10,20] and FPU [21] lattices. Typically, this spontaneous energy localization was observed to occur in two steps. In the first step, a large number of small breathers are created as a result of the modulational instability [9,10,22,23] of travelling plane waves occurring for certain wave number regimes. The second step proceeds by inelastic collisions between the breathers, in which systematically the big breathers grow at expense of the smaller ones. Thus, the outcome will be a small number of large breathers, together with some remaining background of small-amplitude (phonon) oscillations. However, it can generally not be concluded from the numerical simulations that this is the true final state of the system, and actually long-time simulations for FPU-chains [21] revealed also a third step, in which the interaction with the phonon oscillations leads to the final destruction of the breather and equipartition of energy. Thus, to elucidate the nature of the final states for typical initial conditions in anharmonic chains, it is necessary to obtain a better understanding of the mechanisms for interactions between breathers and small-amplitude perturbations.

In this paper, we take the following approach. As initial state, we consider an exact single-site breather solution, and add a small perturbation corresponding to a time-periodic eigensolution to the equations of motion linearized around the breather. These solutions, which can be either localized or extended in space, constitute a complete set in which an arbitrary initial perturbation can be expanded. The localized solutions correspond to internal modes of the breather [13,24–26], while the excitation of an extended solution corresponds to a standing-wave (i.e., non-propagating) phonon interacting with the breather. In Sec. II we describe the model and outline the perturbational approach which forms the analytical backbone for the interpretation of the numerical results presented in Secs. III and IV. Sec. III discusses the long-time consequences of the interaction between the breather and its internal modes, while Sec. IV concerns the interaction between the breather and small-amplitude standing-wave phonons of different wave vectors. We will find that in both cases, a simple argument based on the conservation laws can be used to obtain a sufficient condition for breather growth. In Sec. V we discuss another type of mechanism for breather growth and destruction which becomes appreciable when the amplitude of the standing wave is non-negligible (and consequently the perturbational approach can be expected to fail), and which has its origin in the recently discovered oscillatory instabilities of the nonlinear standing-wave phonon themselves [27]. Finally, we make some concluding remarks in Sec. VI.

Concerning the numerical simulations of the dynamics presented in this paper, unless otherwise stated they always apply for a system of infinite size (finite size systems are considered only in Sec. V). The simulations have been performed either by using very large system sizes or by appending damping regions of various sizes to the boundaries; in all cases we have carefully checked that the boundary conditions have no essential influence on our results.

II. MODEL AND FRAMEWORK FOR THE PERTURBATIONAL APPROACH

A. Model

We consider the following form of the DNLS Hamiltonian with canonical conjugated variables $\{i\psi_n\}, \{\psi_n^*\}$:

$$\mathcal{H}\left(\{i\psi_n\},\{\psi_n^*\}\right) = \sum_n \left(C|\psi_{n+1}-\psi_n|^2 - \frac{1}{2}|\psi_n|^4 \right) \equiv \sum_n \mathcal{H}_n. \tag{1}$$

This yields the DNLS equation

$$i\dot{\psi}_n = \frac{\partial \mathcal{H}}{\partial \psi_n^*} = -C(\psi_{n+1}+\psi_{n-1}-2\psi_n) - |\psi_n|^2\psi_n, \tag{2}$$

which, in addition to the Hamiltonian (1), also conserves the total *excitation norm* (or *power* in nonlinear optics applications),

$$\mathcal{N} = \sum_n |\psi_n|^2 \equiv \sum_n \mathcal{N}_n. \tag{3}$$

The conservation laws for the norm and Hamiltonian are, through Noether's theorem, related to the invariance of the DNLS equation (or, more precisely, of its corresponding action integral) under infinitesimal transformations in phase

($\psi_n \to \psi_n e^{i\epsilon}$) and time ($t \to t+\epsilon$), respectively. Defining the 'norm density' $\mathcal{N}_n$ and 'Hamiltonian density' $\mathcal{H}_n$ as in Eqs. (3) resp. (1), the conservation laws can be expressed in terms of continuity equations as

$$\frac{\mathrm{d}\mathcal{N}_n}{\mathrm{d}t} + (J_\mathcal{N})_n - (J_\mathcal{N})_{n-1} = 0, \tag{4}$$

$$\frac{\mathrm{d}\mathcal{H}_n}{\mathrm{d}t} + (J_\mathcal{H})_n - (J_\mathcal{H})_{n-1} = 0, \tag{5}$$

with the *(norm) current density*

$$J_\mathcal{N} = 2C\mathrm{Im}\left[\psi_n^*\psi_{n+1}\right] \tag{6}$$

and the *Hamiltonian flux density*

$$J_\mathcal{H} = -2C\mathrm{Re}\left[\dot{\psi}_{n+1}(\psi_{n+1}^* - \psi_n^*)\right], \tag{7}$$

respectively. These conservation laws are discrete analogs to those existing for the continuous NLS equations with general nonlinearities (see e.g. [28]), however there is no discrete counterpart to the momentum conservation law since the discrete equation has no continuous translational symmetry in space. Furthermore, we note that the transformation $C \to -C$ in (2) is equivalent to $\psi_n \to (-1)^n e^{-i4Ct}\psi_n$, and thus we will for the rest of this paper only consider $C > 0$ without loss of generality.

The single-site DNLS-breather is a stationary-state solution to Eq. (2) of the form

$$\psi_n(t) = \phi_n(\Lambda)e^{i\Lambda t}, \tag{8}$$

where the time-independent shape $\{\phi_n\}$ depends on the frequency Λ and is spatially localized with a single maximum at a lattice site. The breather exists for all $\Lambda/C > 0$; the limit $C \to 0$ (or $\Lambda \to \infty$) corresponding to the anticontinuous limit, where $\{\phi_n\}$ is localized at a single lattice-site, while the limit $\Lambda/C \to 0$ corresponds to the continuous limit, where $\{\phi_n\}$ approaches the NLS soliton. The single-site breather is a ground state solution to Eq. (2) in the sense that it minimizes the Hamiltonian (1) for a fixed value of the norm (3), i.e., $\delta\mathcal{H} + \Lambda\delta\mathcal{N} = 0$, where the frequency Λ appears as the Lagrange multiplier (see e.g. [15]). The norm for the single-site breather, $\mathcal{N}_\phi$, is known to be a monotonously increasing function of Λ, while the Hamiltonian, $\mathcal{H}_\phi$, is negative and monotonously decreasing (see e.g. [29,30]). From the minimization condition, these functions will be related as

$$\frac{\mathrm{d}\mathcal{H}_\phi}{\mathrm{d}\Lambda} = -\Lambda\frac{\mathrm{d}\mathcal{N}_\phi}{\mathrm{d}\Lambda}. \tag{9}$$

To describe the dynamics close to the breather (8), we introduce the following perturbation expansion:

$$\psi_n(t) = \left\{\phi_n + \lambda\epsilon_n(t) + \lambda^2\eta_n(t) + \lambda^3\xi_n(t) + \lambda^4\theta_n(t) + ...\right\} e^{i\int \Lambda dt}, \tag{10}$$

where $\epsilon_n(0)$ is the initial perturbation and $\eta_n(0) = \xi_n(0) = \theta_n(0) = ... = 0$. Thus, as for the usual stability analysis of stationary states (see e.g. [12,31]), the perturbation is applied in a frame rotating with the breather frequency Λ. Substituting into Eq. (2) and identifying coefficients for consecutive powers of the small parameter λ yields an infinite set of equations, which from 0th to 4th order read:

$$-\Lambda\phi_n + C(\phi_{n+1} + \phi_{n-1} - 2\phi_n) + |\phi_n|^2\phi_n = 0 \tag{11}$$

$$\mathcal{L}(\Lambda)\cdot\{\epsilon_n\} \equiv \{i\dot{\epsilon}_n + C(\epsilon_{n+1} + \epsilon_{n-1} - 2\epsilon_n) + 2|\phi_n|^2\epsilon_n + \phi_n^2\epsilon_n^* - \Lambda\epsilon_n\} = 0 \tag{12}$$

$$\mathcal{L}(\Lambda)\cdot\{\eta_n\} = -\phi_n^*\epsilon_n^2 - 2\phi_n|\epsilon_n|^2 \tag{13}$$

$$\mathcal{L}(\Lambda)\cdot\{\xi_n\} = -2\phi_n^*\epsilon_n\eta_n - 2\phi_n\left(\epsilon_n^*\eta_n + \epsilon_n\eta_n^*\right) - |\epsilon_n|^2\epsilon_n \tag{14}$$

$$\mathcal{L}(\Lambda)\cdot\{\theta_n\} = -2\phi_n\left(\epsilon_n\xi_n^* + \epsilon_n^*\xi_n + |\eta_n|^2\right) - \phi_n^*\left(2\epsilon_n\xi_n + \eta_n^2\right) - \epsilon_n^2\eta_n^* - 2|\epsilon_n|^2\eta_n, \tag{15}$$

where the operator $\mathcal{L}(\Lambda)$ (which is linear over the field of real numbers) is defined from the first equality in Eq. (12). The 0th order equation (11) gives the breather shape $\{\phi_n\}$ (which for the single-site breather can be assumed real and positive without loss of generality), while the 1st order equation (12) is the linearization of the DNLS equation around the breather.

B. Solutions to the linearized equations

To obtain the solutions to the linearized equations (12), we proceed in a similar way as is usually done for continuous generalized NLS models (see e.g. [32–34]) and introduce a substitution of the form

$$\epsilon_n(t) \equiv \epsilon_n^{(r)}(t) + i\epsilon_n^{(i)}(t) = \frac{1}{2}a\,(U_n + W_n)\,e^{-i\omega_p t} + \frac{1}{2}a^*\,(U_n^* - W_n^*)\,e^{i\omega_p t}, \tag{16}$$

so that

$$\epsilon_n^{(r)}(t) = \mathrm{Re}\,(\epsilon_n(t)) = \mathrm{Re}\left(aU_n e^{-i\omega_p t}\right)\ ,\ \epsilon_n^{(i)}(t) = \mathrm{Im}\,(\epsilon_n(t)) = \mathrm{Im}\left(aW_n e^{-i\omega_p t}\right). \tag{17}$$

Substituting (16) into Eq. (12) and assuming ϕ_n real yields

$$\mathcal{L}_0 W_n \equiv -C(W_{n+1} + W_{n-1} - 2W_n) - \phi_n^2 W_n + \Lambda W_n = \omega_p U_n \tag{18}$$

$$\mathcal{L}_1 U_n \equiv -C(U_{n+1} + U_{n-1} - 2U_n) - 3\phi_n^2 U_n + \Lambda U_n = \omega_p W_n, \tag{19}$$

where the operators $\mathcal{L}_0$ and $\mathcal{L}_1$ are Hermitian. Thus, we can obtain the eigenfrequencies ω_p and the corresponding eigenvectors $(\{U_n\},\{W_n\})$ from matrix diagonalization,

$$\mathbf{M}^{(0)} \cdot \begin{pmatrix} \{U_n\} \\ \{W_n\} \end{pmatrix} \equiv \begin{pmatrix} 0 & \mathcal{L}_0 \\ \mathcal{L}_1 & 0 \end{pmatrix} \begin{pmatrix} \{U_n\} \\ \{W_n\} \end{pmatrix} = \omega_p \begin{pmatrix} \{U_n\} \\ \{W_n\} \end{pmatrix}. \tag{20}$$

To make connection to earlier work [2,8], we remark that the vector $\left(\{\epsilon_n^{(r)}\},\{\epsilon_n^{(i)}\}\right) = (\{U_n\},\{-iW_n\})$ is an eigenvector of the Floquet matrix with eigenvalue $e^{-i\omega_p T}$, where the time-period T here is arbitrary since the operators $\mathcal{L}_0$ and $\mathcal{L}_1$ are time-independent. (The symplectic Floquet matrix is $e^{\mathbf{M}_F T}$, where $\mathbf{M}_F$ is obtained from $\mathbf{M}^{(0)}$ by changing $\mathcal{L}_1$ into $-\mathcal{L}_1$.) Thus, (16) is the linear combination of two complex conjugated Floquet eigensolutions which makes $\epsilon_n^{(r)}$ and $\epsilon_n^{(i)}$ real. For the single-site breather, all eigenvalues ω_p of $\mathbf{M}^{(0)}$ are always real, implying the linear stability of the breather for all parameter values $\Lambda/C > 0$ [35]. Accordingly, we can also choose the eigenvectors $(\{U_n\},\{W_n\})$ of $\mathbf{M}^{(0)}$ to be real and normalized, in which case the phase of the amplitude a describes the symmetry properties of the solution (16) under time reversal: choosing a real yields a time-symmetric solution, $\epsilon_n(t) = \epsilon_n^*(-t)$, while choosing a purely imaginary yields a time-antisymmetric solution, $\epsilon_n(t) = -\epsilon_n^*(-t)$.

For an infinite system, the spectrum of the (non-Hermitian) matrix $\mathbf{M^{(0)}}$ can generally be divided into a continuous (phonon) part, corresponding to extended eigenvectors, and a point spectrum corresponding to localized eigenvectors. The phonon spectrum for any localized solution $\{\phi_n\}$ is easily obtained from the limit $|n| \to \infty$, since the condition $\phi_n \to 0$ implies that the operators $\mathcal{L}_0$ and $\mathcal{L}_1$ become identical and Eqs. (18) - (19) reduce into two uncoupled equations for the linear combinations $a_n \equiv U_n + W_n$ resp. $b_n \equiv U_n - W_n$. Assuming $a_n \sim e^{\pm i q_a n}$ and $b_n \sim e^{\pm i q_b n}$, respectively, yields the dispersion relations

$$\omega_p = \Lambda - 2C(\cos q_a - 1), \tag{21}$$

$$\omega_p = -\Lambda + 2C(\cos q_b - 1), \tag{22}$$

from Eqs. (18) - (19). Thus, the continuous spectrum of the matrix $\mathbf{M^{(0)}}$ consists of two branches, symmetrically located around $\omega_p = 0$, and since $\Lambda > 0$ for the single-site breather these two branches never overlap. Note also that two eigenvectors with eigenvalues $\pm\omega_p$ correspond to the same solution to Eq. (12) (changing the sign of ω_p in Eq. (16) is equivalent to changing $U_n \leftrightarrow U_n^*$, $W_n \leftrightarrow -W_n^*$, $a \leftrightarrow a^*$), and therefore it is enough to consider e.g. $\omega_p > 0$, in which case $b_n = U_n - W_n$ always vanishes exponentially as $n \to \pm\infty$.

When Λ/C is not too large, the linear spectrum around the single-site breather contains also two pairs of nonzero isolated eigenvalues ω_p, which correspond to the two internal modes of the breather [13,26]. One of these modes is a spatially symmetric, 'breathing', mode, while the other is a spatially antisymmetric, 'translational' or 'pinning' mode. Numerically, it has been found that the breathing mode exists for $0 < \Lambda/C \lesssim 1.7$, while the pinning mode exists for $0 < \Lambda/C \lesssim 1.1$. The numerically calculated internal mode frequencies ω_p as a function of breather frequency Λ are shown in Fig. 1. Note that as $\Lambda/C \to 0$, the breathing mode frequency approaches the lower edge of the phonon band (but always stays outside the band [26]), while the pinning mode frequency approaches zero (but always stays nonzero). This is consistent with the fact that the soliton solution of the continuous NLS equation has no breathing mode (due to its exact integrability), and has a translational mode with zero frequency due to the translational symmetry of the NLS equation.

To obtain a complete set of solutions to Eq. (12) in which an arbitrary initial perturbation $\epsilon_n(0)$ can be expanded, we must include also the zero-frequency solutions, which generally can be written as a superposition of two fundamental modes. One of these modes ('phase mode' [36]) is the solution $W_n = \phi_n$ to the homogeneous equation (18), $\mathcal{L}_0 W_n = 0$. The corresponding perturbation $\epsilon_n = i\phi_n$ describes a rotation of the overall phase of the breather. The second mode ('growth mode' [36]) is obtained by solving the inhomogeneous equation $\mathcal{L}_1 U_n = -\phi_n$, which has the solution $U_n = \partial\phi_n/\partial\Lambda$. The corresponding solution to Eq. (12) is $\epsilon_n = \partial\phi_n/\partial\Lambda + i\phi_n t$, and corresponds to a time-linear growth of the perturbation representing a small change in the breather frequency.

Although the set of eigensolutions (16) together with the two zero-frequency modes forms a basis for the space of solutions to Eq. (12) (there are no bifurcations, which could result in additional 'marginal modes' [36] with time-linear growth at degenerate eigenvalues), this basis is in general not orthogonal using the ordinary scalar product, and typically there is a considerable overlap between the solution corresponding to the internal breathing mode and the zero-frequency modes. However, in analogy with e.g. [32–34], we can define a 'pseudo-scalar' product between any two vectors $\left(\{U_n^{(1)}\},\{W_n^{(1)}\}\right)$ and $\left(\{U_n^{(2)}\},\{W_n^{(2)}\}\right)$ by

$$\sum_n \left(U_n^{(1)} W_n^{(2)^*} + W_n^{(1)} U_n^{(2)^*}\right). \tag{23}$$

This product is formally not a true scalar product, since for the general case the product of a vector with itself as defined by (23) is not necessarily positive. However, when $(\{U_n\},\{W_n\})$ is a real eigenvector of $\mathbf{M^{(0)}}$ we have $\sum_n U_n W_n = \frac{1}{\omega_p}\sum_n W_n \mathcal{L}_0 W_n$ from (18), and the operator $\mathcal{L}_0$ is positive definite for all $W_n \neq \phi_n$ [35]. With this product, it follows from (18) - (19) that all eigensolutions with different (real) eigenfrequencies ω_p are 'orthogonal' in the sense that

$$\left(\omega_p^{(1)} - \omega_p^{(2)}\right)\sum_n \left(U_n^{(1)} W_n^{(2)^*} + W_n^{(1)} U_n^{(2)^*}\right) = 0, \tag{24}$$

and the only nonzero product involving the zero-frequency modes is the cross-product between the phase mode and the growth mode [35]:

$$\sum_n \phi_n \frac{\partial\phi_n}{\partial\Lambda} = \frac{1}{2}\frac{\mathrm{d}\mathcal{N}_\phi}{\mathrm{d}\Lambda} > 0, \tag{25}$$

where $\mathcal{N}_\phi$ is the norm (3) of the breather with frequency Λ. We also remark that, since the product (23) multiplied by a factor i is just the symplectic product between the two vectors $\left(\{\epsilon_n^{(r)(1)}\},\{\epsilon_n^{(i)(1)}\}\right)$ and $\left(\{\epsilon_n^{(r)(2)}\},\{\epsilon_n^{(i)(2)}\}\right)$, the sign of the product of an eigenvector with itself can be interpreted as the negative of the Krein signature of the corresponding pair of Floquet eigenvalues [2].

C. Strategy for the perturbational approach

We now consider as initial state a single-site breather perturbed in the direction of a single eigenmode (16) (localized or extended) of the linearized equations (12), and wish to describe qualitatively the long-time effects of this perturbation using the expansion (10). In general, taking into account terms up to order p in this expansion yields a solution to the DNLS equation which is correct to $O(\lambda^{p+1})$, i.e., for long but finite time-scales for small initial perturbations (note that the expansion parameter λ plays the same role as the mode amplitude a.). As is wellknown however, this kind of expansion in general diverges due to resonances between solutions to the homogeneous equation (12) and the inhomogeneous terms appearing in the right-hand sides of Eqs. (13)-(15) and the corresponding higher-order equations. A resonance with a solution belonging to the continuous spectrum results in a bounded but nonlocalized solution corresponding to outgoing radiation, while a resonance with an eigenfunction belonging to the discrete spectrum gives a spatially localized response which diverges linearly in time. However, up to any finite order these divergences can be systematically removed by allowing a slow time dependence of the independent variables, which in our case are taken to be the mode amplitude a and the breather frequency Λ. This procedure adds additional terms to the equations, which can be tuned so that the divergent parts of the response disappear. In other words, these two quantities are used as collective variables which, together with the outgoing radiation fields, are expected to describe the main features of the asymptotic dynamics if the initial perturbation is sufficiently small.

The second order correction is given by the inhomogeneous Eq. (13), which with the substitution (16) becomes (choosing ϕ_n, U_n, and W_n real without loss of generality):

$$\mathcal{L}(\Lambda)\cdot\{\eta_n\} = -\frac{1}{2}\phi_n\left[|a|^2\left(3U_n^2+W_n^2\right)+\left(3U_n^2-W_n^2\right)\mathrm{Re}\left(a^2e^{-2i\omega_p t}\right)\right.$$
$$\left.+2iU_nW_n\mathrm{Im}\left(a^2e^{-2i\omega_p t}\right)\right]. \quad (26)$$

Thus, the right-hand side contains one static part and one part involving the frequencies $\pm 2\omega_p$. It acts as a periodic force with frequencies 0 and $2\omega_p$, and since all terms contain the factor ϕ_n this force is localized at the breather region. The response to this force will remain bounded and localized unless the corresponding homogeneous equation (12) has a solution with frequency 0 resp. $2\omega_p$ which is non-orthogonal to the corresponding part of the right-hand side in (26). As will be shown in Sec. III B, a non-zero overlap between the static part of (26) and the zero-frequency solutions of (12) yields a (time-independent) shift of the breather frequency. Moreover, if $\Lambda < 2|\omega_p| < \Lambda + 4C$, so that $2\omega_p$ is inside the phonon band of the homogeneous equation, a resonance will generally occur, resulting in radiation with frequency $2\omega_p$ emitted from the breather region. The strength of the radiation field is determined by the (generally nonzero) overlap between the $2\omega_p$-part of (26) and the corresponding homogeneous solution (see Sec. III B). In a similar way, we obtain that the right-hand-side of the third order equation (14) contains the frequencies ω_p and $3\omega_p$, the fourth order equation (15) contains the frequencies 0, $2\omega_p$, and $4\omega_p$, and in general the pth order equation contains as its highest harmonic the frequency $p\omega_p$. Accordingly, we conclude that if

$$\Lambda < p|\omega_p| < \Lambda + 4C, \quad (27)$$

so that $p\omega_p$ belongs to the phonon band, the perturbed breather will radiate to pth order. The consequences of this radiation for the breather itself will be discussed in Secs. III and IV for the cases of localized and extended perturbations $\{\epsilon_n\}$, respectively.

III. BREATHER INTERACTING WITH INTERNAL MODES

With the initial perturbation $\epsilon_n(0)$ of the single-site breather corresponding to a spatially localized eigenmode of the linearized equations (12), it is clear from the discussion in Sec. II C that higher order radiation always will be created, since for any internal mode frequency ω_p there is always an integer p such that $p\omega_p$ belongs to the phonon band and (27) is fulfilled. Moreover, from the numerical results presented in Fig. 1 we find that the spatially symmetric breathing mode always radiates to second order, since (27) always is fulfilled for $p = 2$, while the antisymmetric pinning mode radiates to second order only when $\Lambda/C \gtrsim 0.480$. Thus, due to this radiation from the breather the total norm contained in any finite region around the breather(i.e., the total norm of breather + internal mode) will always decrease with time. However, the main concern here is the long-time effect of the internal-mode excitation on the breather itself, and thus we must investigate whether there will also be some transfer of energy between the breather and its internal mode. We will first (Sec. III A) show results from direct numerical integration of Eq. (2); then we will give two alternative approaches to the analytical interpretation of these results based on the higher-order equations (13)-(15) (Sec. III B) resp. the conservation laws (4)-(5) (Sec. III C).

A. Numerical simulations

In Fig. 2, we show a typical example on the long-time evolution of a breather when the initial perturbation is taken in the direction of its internal breathing mode. As is seen from Fig. 2 (a), the amplitude of the breathing mode decays slowly with time as a consequence of the losses due to generation of second order radiation, and a careful study of its envelope $|a(t)|$ indicates that it decays as

$$|a(t)| \sim \frac{|a(0)|}{\sqrt{1+\gamma|a(0)|^2\,t}}, \quad (28)$$

where $\gamma > 0$ is a constant. This is consistent with a similar result obtained for the continuum NLS equation with generalized (non-cubic) nonlinearity [33]; the analytical motivation for this result (which is analogous to that of the continuum model given in Ref. [33]) is given in the following subsections.

However, the main result of this section is illustrated in Fig. 2 (b) and (c). Fig. 2 (b) is obtained by calculating the time-average of the central-site intensity as

$$\left\langle|\psi_{n_0}|^2\right\rangle_{t=t_K} = \frac{1}{K}\sum_{k=1}^{K}|\psi_{n_0}(t_k)|^2, \quad (29)$$

where t_k is a set of closely spaced time-instants. It is clear that the interaction between the breather and its internal mode asymptotically leads to an *increase* of the average peak intensity, i.e., to *breather growth*. The same phenomenon is illustrated also in Fig. 2 (c), where we have plotted the difference between the instantaneous breather frequency calculated at time t, $\Lambda(t)$, and the frequency of the unperturbed breather Λ_0. From this figure, we can also conclude that there are two different mechanisms causing the shift of breather frequency. Firstly, there is an initial (almost instantaneous) rather large frequency shift, which can be interpreted as an adaption of the initially perturbed breather to the breather which is 'closest' to the initial condition. As is shown below in Sec. III B, this time-independent frequency shift, which is observed to be always positive for the breathing mode, is a consequence of the overlap between the static part of the right-hand side of the second-order equation (26) and the zero-frequency modes. Secondly, there is the slow, continuous increase of the breather frequency which corresponds to the slow increase of $\left\langle |\psi_{n_0}|^2 \right\rangle_t$ in Fig. 2 (b), indicating a continuous transfer of norm from the internal mode to the breather. It is described by the static part of the right-hand side of the fourth-order equation (15) (see Sec. III B).

When the initial perturbation of the breather is taken in the direction of its internal pinning mode we observe, just as for the breathing mode, that the breather-internal mode interaction asymptotically *always leads to breather growth*. An example is shown in Fig. 3, where the parameter values have been chosen so that the lowest harmonic that enters the phonon band is $3\omega_p$ ($\Lambda/C = 0.45 < 0.480$), We observe two qualitative differences compared to the case with breathing mode excitation. Firstly, since in this case the first phonon resonance occurs only in the third order equation (14), the decay of the internal mode amplitude will be slower, and a good fit is obtained by $|a(t)| \sim |a(0)| \left(1 + \gamma |a(0)|^4 t\right)^{-1/4}$. This agrees with the general result when $p\omega_p$ is the lowest harmonic that enters the phonon band obtained for the continuum generalized NLS equation in Ref. [33]; the derivation of the corresponding result for the discrete case (see Eq. (47)) is given in Sec. III C. As a consequence of the slower decay of the internal mode amplitude, the breather growth will also be slower when $p > 2$, as can be seen from Fig. 3 (c) by comparing the time-scales with those of Fig. 2. Secondly, the initial shift of the breather frequency for a pinning mode excitation is always much smaller than for the breathing mode excitation (also when $2\omega_p$ is in the phonon band), and is when $\Lambda/C \gtrsim 0.55$ also observed to be negative. The explanation for this is given in Sec. III B. However, it is important to stress that also in the cases where the initial frequency shift is negative, we find that the continuous breather growth always will give an asymptotic frequency shift which is positive.

B. Analysis of higher-order equations

Here, we will analyze the higher-order equations (13)-(15) by making use of the strategy of systematically removing the appearing divergent parts as outlined in Sec. II C (in analogy with the treatment of the continuous NLS-type equations in e.g. Refs. [32–34]). First, we show how the dominating contribution to the time-independent frequency shift observed in the numerical simulations above can be calculated from the static part of the right-hand side of the second-order equation (13). This frequency shift can be explicitly taken into account by replacing Λ in Eq. (10) with $\Lambda_0 + \lambda^2 \Lambda_2$, where Λ_0 is the unperturbed breather frequency and Λ_2 the second-order shift to be determined. This implies that the additional term $\Lambda_2 \phi_n$ will be added to the right-hand side of Eq. (26). Writing the response to the static part of (26) as $\eta_n^{(s)} = |a|^2 (u_n^{(s)} + i w_n^{(s)})$ with real $u_n^{(s)}$ and $w_n^{(s)}$ then yields

$$\mathbf{M}^{(0)} \cdot \begin{pmatrix} \left\{ u_n^{(s)} \right\} \\ \left\{ w_n^{(s)} \right\} \end{pmatrix} = \begin{pmatrix} \{0\} \\ \left\{ -\phi_n \left(\frac{\Lambda_2}{|a|^2} - \frac{1}{2} \left(3U_n^2 + W_n^2 \right) \right) \right\} \end{pmatrix}, \tag{30}$$

with $\mathbf{M}^{(0)}$ as defined by Eq. (20). If the expansion of the right-hand side of (30) in the complete set of vectors consisting of the eigenvectors of $\mathbf{M}^{(0)}$ (including the phase mode) and the growth mode contains some component on either of the two zero-frequency modes, the response $\eta_n^{(s)}$ will not remain bounded but diverge linearly with time. Thus, in order to remove this divergency, the frequency shift Λ_2 must be chosen so that both these components are identically zero. The component on the growth mode is trivially zero, while the component on the phase mode is obtained by applying the pseudo-scalar product (23) with the vector corresponding to the growth mode and using (25). Demanding this component to be zero yields

$$\Lambda_2 = \frac{|a|^2}{\frac{\mathrm{d}\mathcal{N}_\phi}{\mathrm{d}\Lambda}} \sum_n \phi_n \frac{\partial \phi_n}{\partial \Lambda} \left(3U_n^2 + W_n^2 \right). \tag{31}$$

This is typically positive for the breathing mode, since the dominating contribution to the sum in (31) comes from the central site n_0, and $\frac{\partial \phi_{n_0}}{\partial \Lambda}$ is always positive. For the spatially antisymmetric pinning mode, there is no contribution to

this sum from the central site, since U_{n_0} and W_{n_0} are zero. The change from a positive to a negative frequency shift when increasing Λ in this case is related to a qualitative change of the nature of the growth mode $\frac{\partial \phi_n}{\partial \Lambda}$: for $\Lambda \gtrsim 0.55$ we find that $\frac{\partial \phi_n}{\partial \Lambda} < 0$ for all $n \neq n_0$, so that all terms in the sum in Eq. (31) are negative, while $\frac{\partial \phi_n}{\partial \Lambda}$ becomes positive also for sites in the neighborhood of n_0 for smaller Λ.

For the rest of the analysis in this subsection, we assume for calculational simplicity that the internal mode frequency is such that $2\omega_p$ is inside the phonon band (and thus it is not applicable for the pinning mode excitation when $\Lambda/C \lesssim 0.480$). Then, the non-static part of the right-hand side of the second order equation (26) will generally give rise to a non-localized response, which can be written in the form $\eta_n^{(rad)} = \frac{1}{2}a^2 \left(u_n^{(2)} + w_n^{(2)}\right) e^{-2i\omega_p t} + \frac{1}{2}a^{*2} \left(u_n^{(2)^*} - w_n^{(2)^*}\right) e^{2i\omega_p t}$. This response corresponds to the radiation field going out from the breather region, and since the right-hand side of (26) is spatially localized and symmetric, this field should asymptotically correspond to two identical linear waves propagating to the left (right) for $n \to -\infty$ $(+\infty)$. Thus, the boundary conditions can be written as

$$u_n^{(2)}, w_n^{(2)} \to r_2 e^{\pm i q_2 n}\ ,\ n \to \pm\infty, \tag{32}$$

with $q_2 = \arccos\left(1 - \frac{2\omega_p - \Lambda}{2C}\right)$ according to (21). Defining for general ω the matrix $\mathbf{M}^{(\omega)}$ (cf. (20)) as

$$\mathbf{M}^{(\omega)} \equiv \begin{pmatrix} -\omega & \mathcal{L}_0 \\ \mathcal{L}_1 & -\omega \end{pmatrix}, \tag{33}$$

the functions $u_n^{(2)}$ and $w_n^{(2)}$ are seen from (26) to be determined by

$$\mathbf{M}^{(2\omega_p)} \cdot \begin{pmatrix} \{u_n^{(2)}\} \\ \{w_n^{(2)}\} \end{pmatrix} = \frac{\phi_n}{2} \begin{pmatrix} \{2U_n W_n\} \\ \{3U_n^2 - W_n^2\} \end{pmatrix}. \tag{34}$$

Since for general ω every eigenvector of $\mathbf{M}^{(\omega)}$ with eigenvalue μ is also an eigenvector of $\mathbf{M}^{(0)}$ with eigenvalue $\mu + \omega$, the right-hand side can be expanded on the basis of eigenvectors of $\mathbf{M}^{(0)}$ (including the zero-frequency modes). The strength of the radiation field is then given by the expansion coefficient for the (continuous spectrum) eigenvector of $\mathbf{M}^{(0)}$ with eigenvalue $2\omega_p$, since this corresponds to the eigenvalue $\mu = 0$ of $\mathbf{M}^{(2\omega_p)}$, and thus a spatially non-bounded response in (34). Using the orthogonality relation (24), this coefficient is simply the 'overlap' between the right-hand side of (34) and the eigenvector of $\mathbf{M}^{(0)}$ with eigenvalue $2\omega_p$ calculated with the pseudo-scalar product (23), which is generally nonzero.

Next, we show how the dominating contribution to the decay of the internal mode amplitude as given by Eq. (28) is obtained from the condition that ξ_n in the third-order equation (14) should remain bounded. To this end, we assume a slow time-dependence of the internal mode amplitude of the form $a = a(\lambda^2 t)$, and consider the response to the terms with frequency ω_p in the right-hand side of Eq. (14) 'corrected' by the additional terms $(-i\dot{a} + \Lambda_2 a)(U_n + W_n)e^{-i\omega_p t} + (-i\dot{a}^* + \Lambda_2 a^*)(U_n - W_n)e^{i\omega_p t}$ appearing as a consequence of including the time-dependence of a and the second-order frequency shift Λ_2 from Eq. (31) in the perturbation expansion (10). Writing the response to this part as $\xi_n^{(\omega_p)} = \frac{1}{2}|a|^2 a \left(u_n^{(3)} + w_n^{(3)}\right) e^{-i\omega_p t} + \frac{1}{2}|a|^2 a^* \left(u_n^{(3)^*} - w_n^{(3)^*}\right) e^{i\omega_p t}$ yields

$$\begin{aligned} &\mathbf{M}^{(\omega_p)} \cdot \begin{pmatrix} \{u_n^{(3)}\} \\ \{w_n^{(3)}\} \end{pmatrix} \\ &= \begin{pmatrix} \{i\frac{\dot{a}}{|a|^2 a} U_n + \phi_n \left(U_n w_n^{(2)} - W_n u_n^{(2)} + 2W_n u_n^{(s)}\right) + \frac{1}{4}\left(U_n^2 W_n + 3W_n^3\right) - \frac{\Lambda_2}{|a|^2} W_n\} \\ \{i\frac{\dot{a}}{|a|^2 a} W_n + \phi_n \left(3U_n u_n^{(2)} + W_n w_n^{(2)} + 6U_n u_n^{(s)}\right) + \frac{1}{4}\left(3U_n^3 + U_n W_n^2\right) - \frac{\Lambda_2}{|a|^2} U_n\} \end{pmatrix}. \end{aligned} \tag{35}$$

A bounded response for $\xi_n^{(\omega_p)}$ exists only if the vector on the right-hand side of (35) has no component in the direction of the internal mode eigenvector $(\{U_n\}, \{W_n\})$, since this is the eigenvector corresponding to the eigenvalue zero of $\mathbf{M}^{(\omega_p)}$. Using the orthogonality relation (24), this component is obtained by application of the product (23) with the vector $(\{U_n\}, \{W_n\})$, and the condition that this component must be zero determines the time-evolution of a. Considering only the absolute value $|a|^2$, the resulting equation has the form $\frac{\mathrm{d}}{\mathrm{d}t}\left(|a|^2\right) + \gamma |a|^4 = 0$, which has the desired solution (28). The constant γ is given by

$$\gamma = \frac{\sum_n \phi_n \left[2U_n W_n \mathrm{Im}\left(w_n^{(2)}\right) + \left(3U_n^2 - W_n^2\right) \mathrm{Im}\left(u_n^{(2)}\right)\right]}{\sum_n U_n W_n} = \frac{8C\omega_p |r_2|^2 \sin q_2}{\sum_n W_n \mathcal{L}_0 W_n} > 0, \tag{36}$$

where the second equality is obtained using Eqs. (18), (32) and (34), and the positivity of γ follows from the fact that, as mentioned in Sec. II B, the operator $\mathcal{L}_0$ is positive definite for all $W_n \neq \phi_n$ [35].

Finally, we show how the continuous increase of the breather frequency appears from the divergent response to the static part of the right-hand side of the fourth-order equation (15). In its unmodified form, this part is given by

$$\begin{aligned} R_n^{(4s)} \equiv -\frac{1}{2}\phi_n|a|^4 \Big\{ & 6U_n \mathrm{Re}\left(u_n^{(3)}\right) + 2W_n \mathrm{Re}\left(w_n^{(3)}\right) + 2iU_n \mathrm{Im}\left(w_n^{(3)}\right) - 2iW_n \mathrm{Im}\left(u_n^{(3)}\right) \\ & + 6(u_n^{(s)})^2 + 3|u_n^{(2)}|^2 + |w_n^{(2)}|^2 + 2i\mathrm{Im}\left(u_n^{(2)*} w_n^{(2)}\right) \Big\} \\ -\frac{1}{4}|a|^4 \Big\{ & 2\left(3U_n^2 + W_n^2\right) u_n^{(s)} + \left(3U_n^2 - W_n^2\right) \mathrm{Re}\left(u_n^{(2)}\right) + 2U_n W_n \mathrm{Re}\left(w_n^{(2)}\right) \\ & - 2iU_n W_n \mathrm{Im}\left(u_n^{(2)}\right) + i\left(U_n^2 - 3W_n^2\right) \mathrm{Im}\left(w_n^{(2)}\right) \Big\}. \end{aligned} \tag{37}$$

Now, it is clear from (31) and (28) that the time-dependence of a will induce a time-dependence of the second-order frequency shift Λ_2 of the form $\Lambda_2(\lambda^2 t)$, so that we can express the total breather frequency up to order λ^4 as $\Lambda(t) = \Lambda_0 + \lambda^2\Lambda_2(\lambda^2 t) + \lambda^4\Lambda_4$, where a 4th order correction Λ_4 has also been included. Then, we must also take into account the time-dependence of the breather shape ϕ_n by writing $\phi_n(\Lambda(t))$. As a consequence, the term $-i\frac{\partial\phi_n}{\partial\Lambda}\dot{\Lambda}_2 + \Lambda_4\phi_n$ will be added to the expression (37) for $R_n^{(4s)}$ in the right-hand side of (15), and writing the response to this total force as $\theta_n^{(s)} = |a|^4\left(u_n^{(4s)} + iw_n^{(4s)}\right)$ with real $u_n^{(4s)}$ and $w_n^{(4s)}$ yields

$$\mathbf{M}^{(0)} \cdot \begin{pmatrix} \{u_n^{(4s)}\} \\ \{w_n^{(4s)}\} \end{pmatrix} = \frac{1}{|a|^4} \begin{pmatrix} \left\{\frac{\partial\phi_n}{\partial\Lambda}\dot{\Lambda}_2 - \mathrm{Im}\left(R_n^{(4s)}\right)\right\} \\ \left\{-\Lambda_4\phi_n - \mathrm{Re}\left(R_n^{(4s)}\right)\right\} \end{pmatrix}. \tag{38}$$

The response $\theta_n^{(s)}$ will be bounded in time only if the right-hand side of (38) has no component either on the growth mode or on the phase mode, which gives two conditions for the determination of $\dot{\Lambda}_2$ and Λ_4. Using (23)-(25), we obtain by demanding the expansion coefficient for the growth mode to be zero:

$$\begin{aligned} \dot{\Lambda}_2 = \frac{|a|^4}{2\frac{\mathrm{d}\mathcal{N}_\phi}{\mathrm{d}\Lambda}} \sum_n \Big\{ & 4\phi_n^2 \left[W_n \mathrm{Im}\left(u_n^{(3)}\right) - U_n \mathrm{Im}\left(w_n^{(3)}\right) + \mathrm{Im}\left(u_n^{(2)} w_n^{(2)*}\right)\right] \\ & + \phi_n \left[2U_n W_n \mathrm{Im}\left(u_n^{(2)}\right) + \left(3W_n^2 - U_n^2\right) \mathrm{Im}\left(w_n^{(2)}\right)\right] \Big\}. \end{aligned} \tag{39}$$

(Similarly, Λ_4 is obtained by demanding the component on the phase mode to be zero.) Thus, the dominating contribution to the frequency growth should be of order $\dot{\Lambda}_2 \sim |a|^4$, so that with the approximate time-dependence (28) of the internal-mode amplitude we obtain qualitatively

$$\Lambda(t) - \Lambda_0 \sim |a(0)|^2 \left(C_1 - C_2 \frac{1}{1 + \gamma|a(0)|^2 t} \right), \tag{40}$$

which is in good agreement with the numerically observed time-dependence of the frequency shift as shown in Fig. 2 (c). However, the positivity of $\dot{\Lambda}_2$ is not easily seen from the expression (39), and therefore we will in the following subsection derive an alternative expression from which the positivity follows immediately, using the conservation laws for the norm resp. Hamiltonian.

C. Approach using conservation laws

We consider first the conservation law (4) for the total norm (3) contained in any large but finite region around the breather. Averaging over a time-interval $[t, t + 2\pi/\omega_p]$ and using Eqs. (10), (16), we can write the time-averaged norm to second order in $|a|$ (putting $\lambda = 1$) as

$$\langle \mathcal{N} \rangle_t(t) \simeq \sum_n \left[\phi_n^2(\Lambda(t)) + \frac{|a(t)|^2}{2}\left(U_n^2 + W_n^2\right)\right]. \tag{41}$$

(Note that there will be no contribution at order 2 from the static second-order correction $u_n^{(s)}$, since the renormalization of the breather frequency Λ according to (31) yields $\sum_n \phi_n u_n^{(s)} = 0$.) In the case when $2\omega_p$ belongs to the phonon band, we obtain the following balance equation, which is correct up to order $|a|^4$:

$$\frac{\mathrm{d}\langle\mathcal{N}\rangle_t}{\mathrm{d}t} = \frac{\mathrm{d}\mathcal{N}_\phi}{\mathrm{d}\Lambda}\dot{\Lambda} + \frac{1}{2}\sum_n \left(U_n^2 + W_n^2\right)\frac{\mathrm{d}|a|^2}{\mathrm{d}t} = J_\mathcal{N}(-\infty) - J_\mathcal{N}(+\infty) = -4C|a|^4|r_2|^2\sin q_2, \tag{42}$$

where we have used Eqs. (4), (6) and (32), and q_2 is as defined below Eq. (32).

Similarly, we can use the conservation law (5) for the Hamiltonian (1) together with the general expression for the Hamiltonian flux density (7) for a small-amplitude plane wave $\psi_n = Ae^{i(qn-\omega(q)t)}$,

$$J_\mathcal{H} = 2|A|^2 C\omega(q)\sin q, \tag{43}$$

to write the balance equation for the total time-averaged Hamiltonian in the same region for the case of second order radiation:

$$\frac{\mathrm{d}\langle\mathcal{H}\rangle_t}{\mathrm{d}t} = \frac{\mathrm{d}\mathcal{H}_\phi}{\mathrm{d}\Lambda}\dot{\Lambda} + \frac{\partial\langle\mathcal{H}\rangle_t}{\partial|a|^2}\frac{\mathrm{d}|a|^2}{\mathrm{d}t} = J_\mathcal{H}(-\infty) - J_\mathcal{H}(+\infty) = -4C|a|^4|r_2|^2(2\omega_p - \Lambda)\sin q_2, \tag{44}$$

which is also correct to order $|a|^4$. The lowest order contribution to the derivative $\frac{\partial\langle\mathcal{H}\rangle_t}{\partial|a|^2}$ can be obtained using the first equality in the equation of motion (2) and its complex conjugate as follows:

$$\begin{aligned}\frac{\partial\langle\mathcal{H}\rangle_t}{\partial|a|^2} &= \frac{1}{a^*}\frac{\partial\langle\mathcal{H}\rangle_t}{\partial a} = \frac{1}{a^*}\sum_n\left\langle\frac{\partial\mathcal{H}}{\partial\psi_n}\cdot\frac{\partial\psi_n}{\partial a} + \frac{\partial\mathcal{H}}{\partial\psi_n^*}\cdot\frac{\partial\psi_n^*}{\partial a}\right\rangle_t \\ &= -\frac{1}{2}\Lambda\sum_n\left(U_n^2 + W_n^2\right) + \omega_p\sum_n U_nW_n + \mathcal{O}(|a|^2),\end{aligned} \tag{45}$$

which is always negative for an internal mode excitation since $|\omega_p| < \Lambda$. Thus, we can combine the two balance equations (42) and (44), and using Eqs. (9) and (45) we obtain the expression (28) for $|a(t)|$ with γ as in (36), together with the following expression for the frequency growth rate from which its positivity is immediately seen:

$$\dot{\Lambda} = \frac{4C|a|^4|r_2|^2\sin q_2}{\frac{\mathrm{d}\mathcal{N}_\phi}{\mathrm{d}\Lambda}}\left(\frac{\sum_n\left(U_n^2+W_n^2\right)}{\sum_n U_nW_n} - 1\right) > 0. \tag{46}$$

This approach also has the advantage that it is easily generalized to the case where the lowest harmonic that enters the phonon band is $p\omega_p$ with $p > 2$, i.e., for the pinning mode excitation when $\Lambda/C \lesssim 0.480$. Then, we can write the boundary conditions at the infinities to lowest order in a as $\psi_n \to a^p r_p e^{i[\pm q_p n - (p\omega_p - \Lambda)t]}$, $n \to \pm\infty$, where $r_p \sim 1$ and $q_p = \arccos\left(\frac{\Lambda - p\omega_p}{2C} + 1\right)$ according to (21). Consequently, we can proceed exactly as above, writing down the balance equations for the norm and Hamiltonian to order $|a|^{2p}$ just by modifying the right-hand sides of Eqs. (42) resp. (44) by replacing $|a|^4$ with $|a|^{2p}$, r_2 with r_p, q_2 with q_p, and $2\omega_p$ with $p\omega_p$. Combining the balance equations yields the following general expression for the time-dependence of the internal mode amplitude,

$$|a(t)| = \frac{|a(0)|}{[1 + (p-1)\gamma_p|a(0)|^{2p-2}t]^{1/(2p-2)}}\ ,\ \gamma_p = \frac{4pC|r_p|^2\sin q_p}{\sum_n U_nW_n} > 0, \tag{47}$$

which is the analog to the expression obtained with similar arguments in [33] for the continuum NLS models. And most importantly, we obtain a general expression for the breather frequency growth rate which is positive for all p:

$$\dot{\Lambda} = \frac{4C|a|^{2p}|r_p|^2\sin q_p}{\frac{\mathrm{d}\mathcal{N}_\phi}{\mathrm{d}\Lambda}}\left(\frac{p\sum_n\left(U_n^2+W_n^2\right)}{2\sum_n U_nW_n} - 1\right) > 0. \tag{48}$$

Thus, integrating Eq. (48) using the time-dependence (47) of the internal-mode amplitude, we obtain that the dominating contribution to the frequency growth generally can be written qualitatively as

$$\Lambda(t) - \Lambda_0 \sim |a(0)|^2\left(C_1 - C_2\frac{1}{1 + (p-1)\gamma_p|a(0)|^{2p-2}\,t}\right)^{1/(p-1)}. \tag{49}$$

Let us finally point out that the approach used in this section provides a simple physical interpretation of why the interaction between the breather and its internal mode in addition to generate radiation also should lead to breather growth. Since the expression (43) for the Hamiltonian flux density of a small-amplitude plane wave is positive when

$\omega(q)$ and q have the same sign, the Hamiltonian energy for a plane wave always propagates in the same direction as the wave itself. Thus, the second (or higher) order radiation emitted from the breather region will always carry away a *positive* amount of the Hamiltonian energy, or, equivalently, negative Hamiltonian energy will flow into the breather region. Moreover, from Eq. (45) it is clear that the contribution to the Hamiltonian from the internal mode always is negative and a monotonously *decreasing* function of its amplitude, and thus the decay of the internal mode would cause an *increase* of the Hamiltonian in the breather region. Consequently, since the Hamiltonian of the pure breather is a monotonously decreasing function of the breather frequency, the breather should grow so that the total Hamiltonian of (breather+internal mode) decreases. A similar mechanism was recently found to cause soliton growth in the parametrically driven continuum NLS equation in the regime of oscillatory instability [34], and this type of argument has also been used to explain the 'quasi-collapse' of a broad excitation to a narrow localized state in the two-dimensional DNLS equation [37].

IV. BREATHER INTERACTING WITH STANDING-WAVE PHONONS

We choose, as in the previous section, the initial perturbation $\epsilon_n(0)$ to be an eigensolution of the linearized equations (12), but now we consider the case of a spatially extended perturbation. Choosing without loss of generality a solution of the form (16) with positive frequency ω_p yields the asymptotic behaviour

$$U_n, W_n \to \cos(qn \pm \delta);\ n \to \pm\infty, \tag{50}$$

where the wave vector q ($0 \le q \le \pi$) is determined by the dispersion relation (21), and δ is the phase shift across the breather. Thus, the excitation of an extended eigenmode corresponds to an interaction between the breather and a non-propagating, standing-wave phonon with small amplitude a. As was mentioned in the introduction, these standing-wave phonons are generally unstable, but since the instabilities become exponentially weak in the small-amplitude limit they are expected to have very little effect on the breather for the perturbation sizes and time-scales considered in this section. We will return to the effects on the breather of these instabilities in Sec. V, where larger perturbations are considered.

In contrast to the case of excitation of a localized internal mode discussed in Sec. III, where higher order radiation always was emitted from the breather region, the condition (27) yields that for the standing-wave perturbation the breather will radiate to higher order only if $\Lambda \le \omega_p < \Lambda/2 + 2C$, so that both ω_p and $2\omega_p$ are inside the phonon band. In terms of the phonon wave vector q, this means that there is a critical value q_c,

$$q_c = \arccos\left(\frac{\Lambda}{4C}\right), \tag{51}$$

such that for $0 \le q < q_c$ second order radiation will be emitted from the breather region, while for $q_c < q \le \pi$ ($\Lambda/2 + 2C < \omega_p \le \Lambda + 4C$) *all* multiples of ω_p are outside the phonon band, and no higher order radiation is emitted. As will be shown below, these two regions yield qualitatively different scenarios for the long-time evolution of the perturbed breather. We also note that for $\Lambda > 4C$ we have $q_c = 0$, so that for the highly localized, high-frequency breathers *no phonons can generate higher-order radiation* (note also that there are no internal modes in this regime). Furthermore, we always have $q_c < \pi/2$, so that the regime of higher-order radiation generation is a subset of the regime $0 < q < \pi/2$ where modulational instability for *travelling* plane waves occurs [9].

Let us first discuss the case $q < q_c$. A typical example of the long-time evolution of a breather interacting with a small-amplitude standing-wave phonon with $q < q_c$ is illustrated by Fig. 4. As is seen from Fig. 4 (a), the amplitude of the oscillations remains essentially constant in time, but a closer inspection reveals that the average value of $|\psi_{n_0}|^2$ asymptotically *increases* with an apparently constant rate (see inset in Fig. 4 (b)). Similarly, Fig. 4 (b) shows that also the total norm contained in any finite region around the breather asymptotically increases linearly with time. We find that these results are generic for all cases when the phonon wave vector $q < q_c$ (the spatial symmetry of the phonon is not important for the asymptotic behaviour), and thus we conclude that in this regime, the breather can 'pump' energy from the phonon (which is infinite for an infinite system), and thereby grow.

In the same spirit as for the internal mode excitation in Sec. III C, we can give a simple argument based on the conservation laws to motivate why the generation of second order radiation should lead to breather growth. To this end, we assume that the initial standing-wave phonon is infinitely extended, and that far away from the breather a stationary regime will be reached corresponding to the following boundary conditions

$$\psi_n \to \left[(ae^{\mp iqn} + re^{\pm iqn})e^{-i\omega_p t} + r_2 e^{i(\pm q_2 n - 2\omega_p t)}\right] e^{i\Lambda t}\ ;\ n \to \pm\infty. \tag{52}$$

Thus, we have taken into account the second-order radiation with frequency $2\omega_p$ generated at the breather region but neglected possible higher-order radiation; moreover the resonance at the original phonon frequency ω_p in the third-order equation (14) has been taken into account by allowing the incoming and outgoing complex amplitudes a and r to be different. We can then, in analogy with Eqs. (42) and (44), write the balance equations for the total norm and Hamiltonian contained in a region around the breather averaged over a time-interval $[t, t + 2\pi/\omega_p]$ as

$$\frac{\mathrm{d}\langle \mathcal{N} \rangle_t}{\mathrm{d}t} = \frac{\mathrm{d}\mathcal{N}_\phi}{\mathrm{d}\Lambda}\dot{\Lambda} = \langle J_{\mathcal{N}}(-\infty)\rangle_t - \langle J_{\mathcal{N}}(+\infty)\rangle_t = 4C\left[(|a|^2 - |r|^2)\sin q - |r_2|^2 \sin q_2\right], \tag{53}$$

and

$$\begin{aligned}\frac{\mathrm{d}\langle \mathcal{H} \rangle_t}{\mathrm{d}t} = \frac{\mathrm{d}\mathcal{H}_\phi}{\mathrm{d}\Lambda}\dot{\Lambda} &= \langle J_{\mathcal{H}}(-\infty)\rangle_t - \langle J_{\mathcal{H}}(+\infty)\rangle_t \\ &= 4C\left[(|a|^2 - |r|^2|)(\omega_p - \Lambda)\sin q - |r_2|^2(2\omega_p - \Lambda)\sin q_2\right],\end{aligned} \tag{54}$$

respectively. Here, we have used the facts that the time-average of the norm current density (6) and the Hamiltonian flux density (7) are additive quantities for small-amplitude plane waves, and that in the stationary regime, the mode amplitudes a, r and r_2 are time-independent. Combining Eqs. (53) and (54) and using (9), we obtain that the breather frequency grows with a constant rate given by

$$\dot{\Lambda} = \frac{4C|r_2|^2 \sin q_2}{\frac{\mathrm{d}\mathcal{N}_\phi}{\mathrm{d}\Lambda}} > 0. \tag{55}$$

The physical interpretation of this result is, similarly as for the case of internal mode excitation, that the generation of higher-order radiation results in a net flow of negative Hamiltonian energy into the breather region, which is absorbed by the breather by increasing its frequency and maximum amplitude. This process is similar to the one observed for the two-channel phonon scattering on breathers in a Klein-Gordon model with a Morse potential in Ref. [38]; however in the latter case the second outgoing wave resulted from a resonance in the linearized equations and were therefore of the same order of magnitude as the incoming wave, and moreover the outcome in this case was breather decay since the energy of a Klein-Gordon breather is an increasing function of its amplitude.

Considering now the regime $q > q_c$ where all multiples of ω_p are outside the phonon band, the most important conclusion from our extensive numerical investigations is that we *never observe breather growth*. Instead, we sometimes (but not always) observe a very slow decrease of $\left\langle |\psi_{n_0}|^2 \right\rangle_t$, and an increase of the fluctuations around this mean-value. This behaviour is illustrated by Fig. 5 (a) and (b). A possible interpretation of these results is that, since the higher harmonics which are created by the breather-phonon interaction cannot propagate, they stay trapped around the breather. Thus, this could lead to a transfer of energy from the 'pure' breather, which acquires more and more internal frequencies and becomes a 'chaotic breather' [21]. Another possible interpretation is that the increase of the oscillation amplitude is connected with the oscillatory instabilities of the standing waves; as we will show in the next section these instabilities provide a mechanism for breather decay. However in some cases, illustrated by Fig. 5 (c) and (d), the oscillation amplitude as well as its average value apparently approaches a constant limit value. We have at present no explanation for this behaviour (as will be discussed in the next section, there exist exact 'phonobreather' solutions which could be candidates for such a final state, but they are unstable); it is possible that the time ranges that we were able to study with sufficient numerical accuracy in these cases simply were too short to observe the scenario described by Fig. 5 (a) and (b).

To conclude this section, we repeat our main result that breather growth is observed if and only if $q < q_c$, where q_c is given by (51). The fact that $q_c = 0$ for $\Lambda > 4C$ thus implies the existence of an upper limit beyond which the breather cannot grow with the type of perturbations considered here. We would also like to relate our results to recent numerical simulations of breathers interacting with *propagating* phonons in Klein-Gordon [39] and FPU [21] lattices. For the Klein-Gordon lattice with a (soft) Morse on-site potential, phonons with small wave vector q were observed to yield breather growth, while phonons with large q caused breather decay. For a FPU lattice with hard anharmonicity, the opposite situation was observed, i.e., small-q phonons caused breather decay and large-q phonons breather growth. The fact that the situation for the hard FPU lattice was opposite to that of the soft Klein-Gordon lattice could be expected, since in the former case the modulational instability occurs for large q, whereas soft Klein-Gordon and DNLS lattices with $C > 0$ are modulationally unstable for small q. However, we stress that the relation between plane-wave modulational instability and breather growth is nontrivial, and at least for the case considered in this paper the critical value q_c for breather growth from interaction with standing-wave phonons differs from the critical value $q = \pi/2$ for modulational instability of travelling waves.

V. BREATHER GROWTH AND DESTRUCTION FROM STANDING-WAVE INSTABILITIES

In this section, with the aim at describing the interaction between a breather and a standing-wave phonon with non-negligible amplitude, we will take a slightly different point of view than in the preceding sections. Instead of choosing as initial condition an exact breather solution and adding a perturbation corresponding to an eigenmode of the linearized equations, we will here consider initial conditions which are exact *phonobreather* [2] (or *nanopteron*) solutions. By definition, a phonobreather consists of a spatially localized breather on top of a spatially extended tail which is a nonlinear, standing-wave phonon. (There are also solutions where the tail is a propagating wave [36], but we will not discuss them further here.) Phonobreathers exist generically for nonlinear lattice-equations (see e.g. [2,6]), but their existence normally requires an integer relationship between the breather and phonon frequencies. However, for the DNLS equation phonobreathers exist for *any* (rational or irrational) relation between the two frequencies [11], as a consequence of the additional invariance of the equation under global phase transformations.

Since the phonobreathers are exact solutions consisting of a breather part and a standing-wave part, one could expect them to be attractors for the initial conditions considered in Sec. IV. However, as was shown recently [27], generically for soft Klein-Gordon and DNLS models with $C > 0$ *all* phonobreathers with phonon wave vector $q \neq \pi$ will be *linearly unstable* if, for fixed phonon amplitude a, the linear coupling C is larger than some threshold value $C_{cr}(a, q)$ (i.e., away from the anticontinuous limit). (For lattices with hard potentials and DNLS with $C < 0$, the stable phonobreather has $q = 0$.) These instabilities are caused by an oscillatory instability of the standing-wave phonon itself, which can be understood by considering the construction of a nonlinear standing wave with wave vector q close to π at the anticontinuous limit $C = 0$ by introducing a periodic array of discommensurations or 'defects' in the nonlinear phonon with wave vector π and amplitude a, $\psi_n = a(-1)^n e^{-i(4C-|a|^2)t}$, which is linearly stable for all a and $C > 0$ [9]. In the anticontinuous limit $C = 0$, each defect consists when $\pi/2 < q < \pi$ of one extra site with $\psi_n = 0$ added to the π-phonon, which consequently suffers an additional phase shift of π across each defect. For $0 < q < \pi/2$, each defect consists of several consecutive zero-amplitude sites with associated phase shifts (a general method for generating the anticontinuous coding sequence for standing-wave phonons from a circle map is described in [27]); in this case it is also useful to consider the periodic repetition of sites with $\psi_n = \pm a$ as defects of the zero-amplitude state.

The limit case of one isolated zero-amplitude defect, which is a discrete counterpart of the dark-soliton solution of the continuum NLS equation, was investigated in [40]. The linear stability analysis of this mode showed that, although it is stable close to the anticontinuous limit, it suffers a bifurcation for $C/|a|^2 = C_c \approx 0.0765$ where two pairs of eigenvalues of the eigenvalue problem (20) go out in the complex plane. The resulting oscillatory instability occurs due to a resonance between a mode localized around the defect (the defect pinning mode) and linear radiation modes. It was shown that for finite systems, the mode recovers its stability above some upper critical value of $C/|a|^2$ (since the wavelength of the resonating linear modes becomes larger than the system size); however this critical value increases with system size so that in the limit of an infinite system, the instability persists for all $C/|a|^2 > C_c$ but with a growth-rate that decreases in an exponential-like fashion when approaching the continuum limit $C/|a|^2 \to \infty$. This instability was shown to result in the defect becoming mobile (in NLS terms, the stationary 'black' soliton with zero minimum intensity transforms into a moving 'grey' soliton with non-zero minimum intensity) and radiation being emitted. In terms of the phase dynamics, this describes a moving, slowly spreading phase kink.

The instability scenario for the standing-wave phonons is basically the same as for the isolated defect, with the essential difference that the localized pinning modes associated with the individual, periodically repeated defects now will form a continuous 'defect band'. In general, the Krein signature [2] of this defect band is opposite to that of the bands associated with the non-zero amplitude sites [27] (for $0 < q < \pi/2$ there are generally several defect bands, but they will have the same Krein signature), and as a consequence resonances between the bands will occur if the linear coupling C is large enough, giving rise to similar oscillatory instabilities as described above (details are given in [27]). We remark that earlier analysis [41] of standing waves in nonlinear lattices, based on a quasi-continuum approximation, did not reveal these instabilities since their origin is the discrete nature of the lattice.

Let us now return to the main objective of this section, namely to study the effect of the oscillatory standing-wave instabilities on the phonobreathers. We find that the families of phonobreathers which are stable close to the anticontinuous limit and whose tails approach harmonic standing waves in the small-amplitude limit can be constructed from anticontinuous standing-wave solutions at $C = 0$, placing the breather at a zero-amplitude site of the phonon and adjusting it so that the resulting solution is either symmetric or antisymmetric around the breather site. Denoting the anticontinuous breather amplitude by b (the phase of the breather site is unimportant when $|b| \neq |a|$ [11]), this yields the following possibilities:
(i) For $q > \pi/2$ the antisymmetric anticontinuous solution (here $q = 2\pi/3$)

$$\{\psi_n(0)\} = \{... - a, a, 0, -a, a, 0, -a, a, b, -a, a, 0, -a, a, 0...\}, \tag{56}$$

with the asymptotic behaviour $\psi_n(0) \sim a\sin(qn), n \to \pm\infty$ in the continuum limit $C/|a|^2 \to \infty$. (Note that this solution is antisymmetric only at $C = 0$.)
(ii) From (56) we can construct a symmetric solution for $q > \pi/2$ by introducing an additional phase shift of π at one side of the breather site, giving for $q = 2\pi/3$

$$\{\psi_n(0)\} = \{...-a, a, 0, -a, a, 0, -a, a, b, a, -a, 0, a, -a, 0...\}, \tag{57}$$

with the asymptotic behaviour $\psi_n(0) \sim a\cos(qn \pm \pi/2), n \to \pm\infty$ in the continuum limit.
(iii) For $q = M\pi/N < \pi/2$, N even, the number of consecutive zero-amplitude sites is odd and the antisymmetric anticontinuous solution is for e.g. $q = \pi/4$

$$\{\psi_n(0)\} = \{...0, 0, 0, a, 0, 0, 0, -a, 0, 0, 0, a, 0, b, 0, -a, 0, 0, 0, a, 0, 0, 0, -a...\} \tag{58}$$

behaving as $\psi_n(0) \sim a\cos(qn), n \to \pm\infty$ in the continuum limit.
(iv) From (58) the symmetric solution for $q = M\pi/N < \pi/2$, N even, is constructed by a phase shift as above, giving for $q = \pi/4$

$$\{\psi_n(0)\} = \{...0, 0, 0, a, 0, 0, 0, -a, 0, 0, 0, a, 0, b, 0, a, 0, 0, 0, -a, 0, 0, 0, a...\} \tag{59}$$

with the asymptotic behaviour $\psi_n(0) \sim -a\sin(qn \pm \pi/2), n \to \pm\infty$ in the continuum limit.
(v) For $q = M\pi/N < \pi/2$, N odd, the number of consecutive zero-amplitude sites is even and we must add an extra site to obtain the antisymmetric anticontinuous solution, which for e.g. $q = \pi/3$ becomes

$$\{\psi_n(0)\} = \{...0, 0, a, 0, 0, -a, 0, 0, a, 0, b, 0, -a, 0, 0, a, 0, 0, -a, 0, 0, a...\} \tag{60}$$

behaving as $\psi_n(0) \sim a\cos(q(n + 1/2) \pm q/2), n \to \pm\infty$ in the continuum limit. (A solution with similar properties is obtained by instead removing one zero-amplitude site; however its symmetric counterpart is always unstable.)
(vi) The symmetric counterpart of (60) for $q = M\pi/N < \pi/2$, N odd, is constructed by a phase shift as above, giving for $q = \pi/3$

$$\{\psi_n(0)\} = \{...0, 0, a, 0, 0, -a, 0, 0, a, 0, b, 0, a, 0, 0, -a, 0, 0, a, 0, 0, -a...\} \tag{61}$$

with the asymptotic behaviour $\psi_n(0) \sim -a\sin(q(n + 1/2) \pm (q + \pi)/2), n \to \pm\infty$ in the continuum limit.

A typical example on the time-evolution for an initially very weakly perturbed phonobreather with phonon wave vector $q > \pi/2$ and phonon amplitude small but non-negligible compared to the breather amplitude is illustrated in Fig. 6. (The example in the figure belongs to type (i), but similar dynamics is observed also for the spatially symmetric states of type (ii).) We can clearly distinguish two different steps leading to the final breather destruction. The first step is the linear oscillatory instability described above, which leads to the generation of new internal frequencies of the breather, and to the movement of the defect sites in a similar way as for the case of an isolated defect. In the second step, the moving defects start interacting, and a close inspection of Fig. 6 (a) shows that neighboring defects tend to merge and create regions of accumulated phase fluctuations travelling around in the lattice. These will interact with the breather, and apparently cause its decay. When the breather has decayed sufficiently to have an excitable pinning mode, it will start to move in the lattice but with rapidly decreasing amplitude, and it will finally be destroyed. We have at present no complete understanding for the mechanism by which the interaction of the breather with the moving 'phase kinks' cause its decay, but we remark that a similar scenario was observed when adding to the DNLS equation an external, parametric white noise term [42]. In that case, the white-noise approximation allowed a qualitative understanding of the breather decay as a consequence of phase fluctuations by using a collective coordinate approach.

However, to observe this scenario for breather destruction it is necessary (at least for a finite system) that the phonon amplitude is not too small compared to the breather amplitude. If we increase the breather amplitude in Fig. 6 (or decrease the phonon amplitude) sufficiently, we find that although the oscillatory instability develops, the fluctuations created in the second step will be too weak to cause the breather to decay, and it will live seemingly forever as a 'chaotic phonobreather'. The absence of decay for small perturbations can be viewed as a consequence of the fact that the single-site DNLS breather is nonlinearly (Lyapunov) stable for norm-conserving perturbations, in the sense that $|\psi_n(t)|$ remains arbitrarily close to the breather for all times if the initial perturbation is small enough [15]. Thus, it is clear that for finite systems, the breather cannot be destroyed unless the phonon amplitude exceeds some critical value, while nothing can be said about the infinite system since any infinitely extended phonon obviously has an infinite norm.

With $0 < q < \pi/2$, the first step resulting from the oscillatory instability occurs in a similar way as for $q > \pi/2$: the breather acquires new frequencies and the small-amplitude sites of the phonon start moving. By instead making

the interpretation that the sites with non-zero amplitude at the anticontinuous limit are defects in the zero-amplitude state, their movement can be seen as a consequence of the repulsive interaction between spatially separated, small-amplitude breathers with opposite phases observed e.g. in [17]. We also observe, similarly as for $q > \pi/2$, the merging of neighboring defects, but in this case their interaction with the breather will not lead to breather decay, but rather to breather growth if the original amplitude of the breather is not too large. A typical example is illustrated in Fig. 7. It can be seen by a careful inspection of Fig. 7 (a) how the merging of small-amplitude sites results in localized humps of larger amplitude reminiscent of small-amplitude moving breathers travelling around in the lattice. The interaction of these humps with the original breather leads to growth of the latter in a similar way as observed in [19–21]. However, this growth stops when the breather amplitude has reached a critical value which is close to (but apparently smaller than) that corresponding to the limit value $\Lambda = 4C$ for small-amplitude perturbations found in Sec. IV (the latter corresponds to $|\psi_{n_0}|^2 \approx 5.65$). The final state appears also here to be a 'chaotic phonobreather'; we have followed the time evolution of this kind of state for times up to 10^6 without seeing any signs of decay. Also, if the initial breather frequency is chosen above the critical value $\Lambda = 4C$, we typically do not observe breather growth; instead the mean value of the chaotic amplitude oscillations resulting from the oscillatory instability remains close to the initial amplitude.

VI. CONCLUDING REMARKS

Investigating the interaction between discrete nonlinear Schrödinger breathers and small perturbations, we have found firstly that exciting an internal mode of the breather always leads to a slow energy transfer to the breather, i.e., to breather growth. Furthermore, we found that a DNLS-breather can pump energy from a small-amplitude standing-wave phonon, provided that the phonon wave vector is smaller than the critical value q_c given by Eq. (51). In both cases, the mechanism for breather growth involves the higher-order generation of radiating modes. Since this mechanism disappears at the threshold value $\Lambda = 4C$ of the breather frequency, it is impossible for a breather to grow beyond this value with the type of small-amplitude perturbations considered here. To analyze the interaction between breathers and standing-wave phonons of small but non-negligible amplitude, we considered the long-time evolution of weakly perturbed exact phonobreather solutions. The instabilities of these, originating in oscillatory instabilities of the nonlinear phonons, where shown to lead to propagating inhomogeneities whose interaction with the breather provided a mechanism for breather decay and destruction (when the phonon wave vector $q > \pi/2$) or growth ($q < \pi/2$ and $\Lambda < 4C$).

As was mentioned already in the introduction, the existence of the two conserved quantities (1) and (3) makes the DNLS equation non-generic among nonlinear lattice equations, and it is therefore necessary to investigate to what extent the results obtained in this paper apply also for Klein-Gordon and FPU lattices. We plan to address these questions in a forthcoming publication, but let us stress already here that the perturbational approach used here for the DNLS equation needs to be modified to account for the fact that generically, the dynamics of the breather involves also higher harmonics of its fundamental frequency. Moreover, the approach used in Secs. III C and IV based on the conservation laws cannot be directly applied in the absence of a second conserved quantity. However, in view of the wide applicability of the DNLS equation (and in particular its appearance as a limit case of general lattice equations as mentioned in the introduction), we believe that the mechanisms for breather growth and destruction described in this paper are essential ingredients also for the corresponding processes in general lattice models.

ACKNOWLEDGMENTS

We thank Yu. S. Kivshar for giving us an early preprint of Ref. [33], I. V. Barashenkov for directing our attention to Ref. [34], and A. M. Morgante for discussions on phonobreathers and standing-wave instabilities. M. J. acknowledges a Marie Curie Research Training Grant from the European Community. A preliminary version of these results was presented at the conference Nonlinearity '99 (Heraklion, May 10-14, 1999).

---

[1] L. D. Landau, Phys. Zeit. Sowjetunion **3**, 664 (1933).
[2] S. Aubry, Physica D **103**, 201 (1997).

[3] S. Flach and C. R. Willis, Phys. Rep. **295**, 181 (1998).
[4] S. Takeno, K. Kisoda, and A. J. Sievers, Prog. Theor. Phys. Suppl. **94**, 242 (1988).
[5] R. S. MacKay and S. Aubry, Nonlinearity **7**, 1623 (1994).
[6] J. L. Marín and S. Aubry, Nonlinearity **9**, 1501 (1996).
[7] T. Dauxois, M. Peyrard, and C. R. Willis, Physica D **57**, 267 (1992); T. Dauxois, M. Peyrard, and A. R. Bishop, Phys. Rev. E **47**, 684 (1993); M. Peyrard, in *Nonlinear Cooperative Phenomena in Biological Systems*, edited by L. Matsson (World Scientific, Singapore, 1998), p. 276, and references therein.
[8] J. L. Marín, S. Aubry, and L. M. Floría, Physica D **113**, 283 (1998).
[9] Yu. S. Kivshar and M. Peyrard, Phys. Rev. A **46**, 3198 (1992).
[10] I. Daumont, T. Dauxois, and M. Peyrard, Nonlinearity **10**, 617 (1997).
[11] M. Johansson and S. Aubry, Nonlinearity **10**, 1151 (1997).
[12] J. C. Eilbeck, P. S. Lomdahl, and A. C. Scott, Physica D **16**, 318 (1985).
[13] M. Johansson, S. Aubry, Yu. B. Gaididei, P. L. Christiansen, and K. Ø. Rasmussen, Physica D **119**, 115 (1998), and references therein.
[14] D. Hennig and G. P. Tsironis, Phys. Rep. **307**, 333 (1999), and references therein.
[15] M. I. Weinstein, Nonlinearity **12**, 673 (1999).
[16] S. M. Jensen, IEEE J. Quantum Electron. **QE-18**, 1580 (1982); D. N. Christodoulides and R. I. Joseph, Opt. Lett. **13**, 794 (1988).
[17] A. B. Aceves, C. De Angelis, T. Peschel, R. Muschall, F. Lederer, S. Trillo, and S. Wabnitz, Phys. Rev. E **53**, 1172 (1996).
[18] H. S. Eisenberg, Y. Silberberg, R. Morandotti, A. R. Boyd, and J. S. Aitchison, Phys. Rev. Lett. **81**, 3383 (1998).
[19] K. Ø. Rasmussen, A. R. Bishop, and N. Grønbech-Jensen, Phys. Rev. E **58**, R40 (1998); K. Ø. Rasmussen, S. Aubry, A. R. Bishop, and G. P. Tsironis, submitted for publication.
[20] T. Dauxois and M. Peyrard, Phys. Rev. Lett. **70**, 3935 (1993); O. Bang and M. Peyrard, Phys. Rev. E **53**, 4143 (1996); M. Peyrard, Physica D **119**, 184 (1998).
[21] T. Cretegny, T. Dauxois, S. Ruffo, and A. Torcini, Physica D **121**, 109 (1998).
[22] T. Cretegny and S. Aubry, Phys. Rev. B **55**, R11929 (1997).
[23] T. Dauxois, S. Ruffo, and A. Torcini, Phys. Rev. E **56**, R6229 (1997).
[24] Ding Chen, S. Aubry, and G. P. Tsironis, Phys. Rev. Lett. **77**, 4776 (1996).
[25] C. Baesens, S. Kim, and R. S. MacKay, Physica D **113**, 242 (1998).
[26] Yu. S. Kivshar, D. E. Pelinovsky, T. Cretegny, and M. Peyrard, Phys. Rev. Lett. **80**, 5032 (1998).
[27] A. M. Morgante, oral communication at the conference *Nonlinearity '99*, Heraklion, 10-14 May 1999, organized by T. Geisel and G. P. Tsironis; A. M. Morgante, G. Kopidakis, M. Johansson, and S. Aubry, in preparation.
[28] J. Juul Rasmussen and K. Rypdal, Physica Scripta **33**, 481 (1986).
[29] A. C. Scott and L. MacNeil, Phys. Lett. **98A**, 87 (1983).
[30] Yu. B. Gaididei, S. F. Mingaleev, P. L. Christiansen, and K. Ø. Rasmussen, Phys. Rev. E **55**, 6141 (1997); K. Ø. Rasmussen, P. L. Christiansen, M. Johansson, Yu. B. Gaididei, and S. F. Mingaleev, Physica D **113**, 134 (1998).
[31] J. Carr and J. C. Eilbeck, Phys. Lett. **109A**, 201 (1985).
[32] D. J. Kaup, Phys. Rev. A **42**, 5689 (1990).
[33] D. E. Pelinovsky, Yu. S. Kivshar, and V. V. Afanasjev, Physica D **116**, 121 (1998).
[34] N. V. Alexeeva, I. V. Barashenkov, and D. E. Pelinovsky, Nonlinearity **12**, 103 (1999).
[35] E. W. Laedke, K. H. Spatschek, and S. K. Turitsyn, Phys. Rev. Lett. **73**, 1055 (1994).
[36] S. Aubry and T. Cretegny, Physica D **119**, 34 (1998).
[37] P. L. Christiansen, Yu. B. Gaididei, V. K. Mezentsev, S. L. Musher, K. Ø. Rasmussen, J. Juul Rasmussen, I. V. Ryzhenkova, and S. K. Turitsyn, Physica Scripta **T67**, 160 (1996).
[38] T. Cretegny, S. Aubry, and S. Flach, Physica D **119**, 73 (1998).
[39] T. Cretegny, *Dynamique collective et localisation de l'énergie dans les réseaux non-linéaires*, Ph. D. Thesis, École normale supérieure de Lyon, France, 1998 (in French).
[40] M. Johansson and Yu. S. Kivshar, Phys. Rev. Lett. **82**, 85 (1999).
[41] Yu. S. Kivshar, M. Haelterman, and A. P. Sheppard, Phys. Rev. E **50**, 3161 (1994).
[42] P. L. Christiansen, Yu. B. Gaididei, M. Johansson, and K. Ø. Rasmussen, Phys. Rev. B **55**, 5759 (1997).

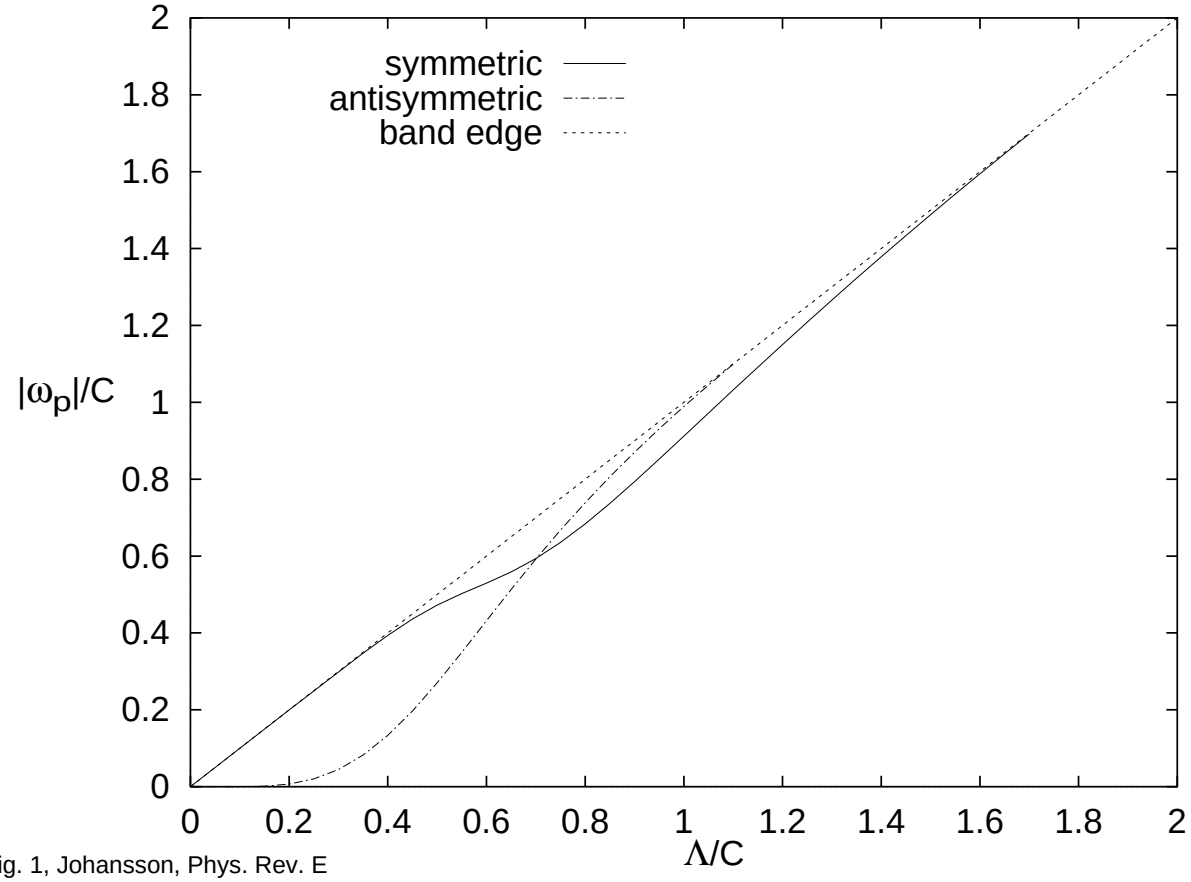

Fig. 1, Johansson, Phys. Rev. E

FIG. 1. Variation of internal mode frequencies versus breather frequency for the spatially symmetric (solid line) resp. antisymmetric (dashed-dotted line) internal modes of the single-site breather. Dashed straight line shows the lower band edge of the phonon band.

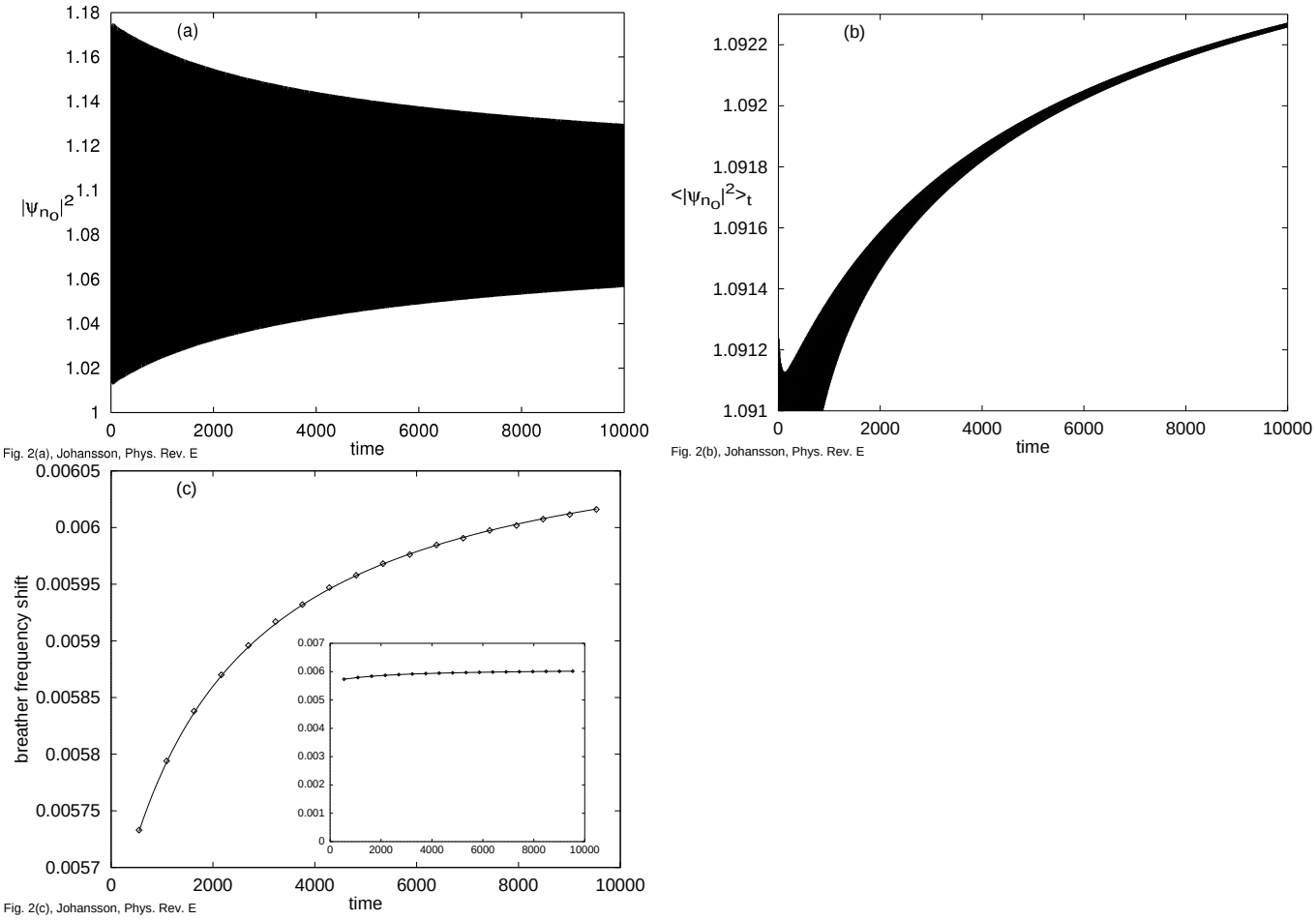

Fig. 2(a), Johansson, Phys. Rev. E

Fig. 2(b), Johansson, Phys. Rev. E

Fig. 2(c), Johansson, Phys. Rev. E

FIG. 2. Time-evolution of a breather with an initial perturbation in the direction of the breathing mode. Parameters are $\Lambda = 0.5$, $\omega_p \approx 0.47$, and $C = 1$. (a) shows the time-evolution of the central-site intensity $|\psi_{n_0}|^2$, (b) shows its time-average $\left\langle |\psi_{n_0}|^2 \right\rangle_t$ calculated using Eq. (29), while (c) shows the instantaneous shift of breather frequency $\Lambda(t) - \Lambda_0$. The solid line in the main figure in (c) is a fit using Eq. (40) with $a(0) = 0.082$, $C_1 = 0.9078$, $C_2 = 0.069$, and $\gamma = 0.067$.

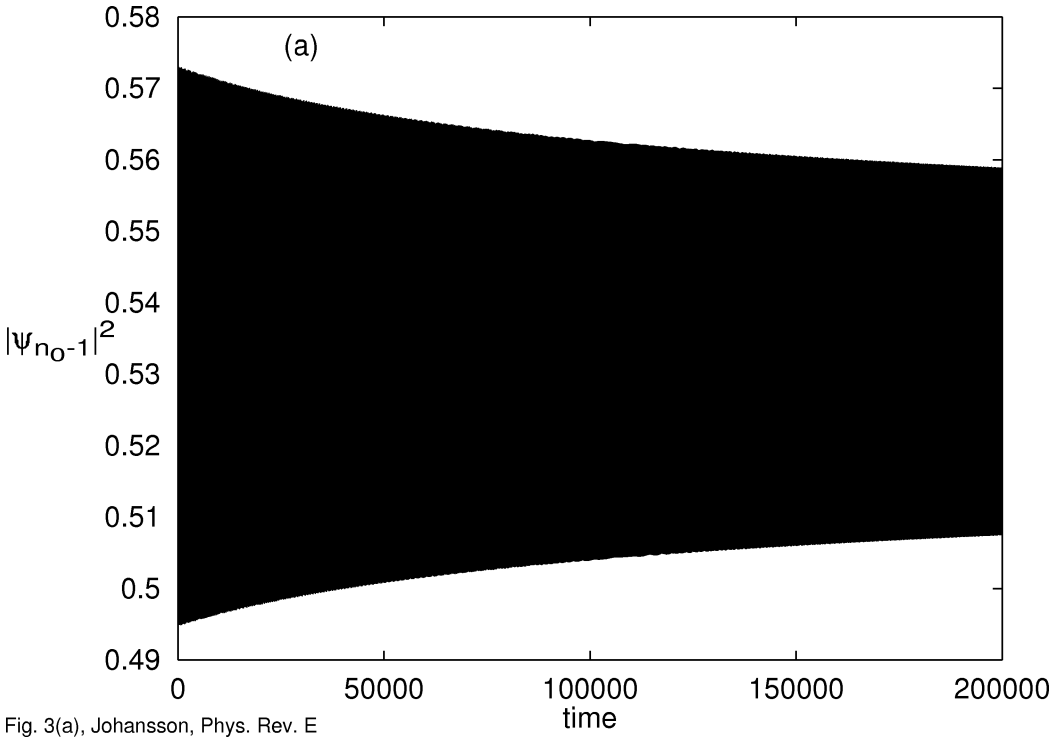

Fig. 3(a), Johansson, Phys. Rev. E

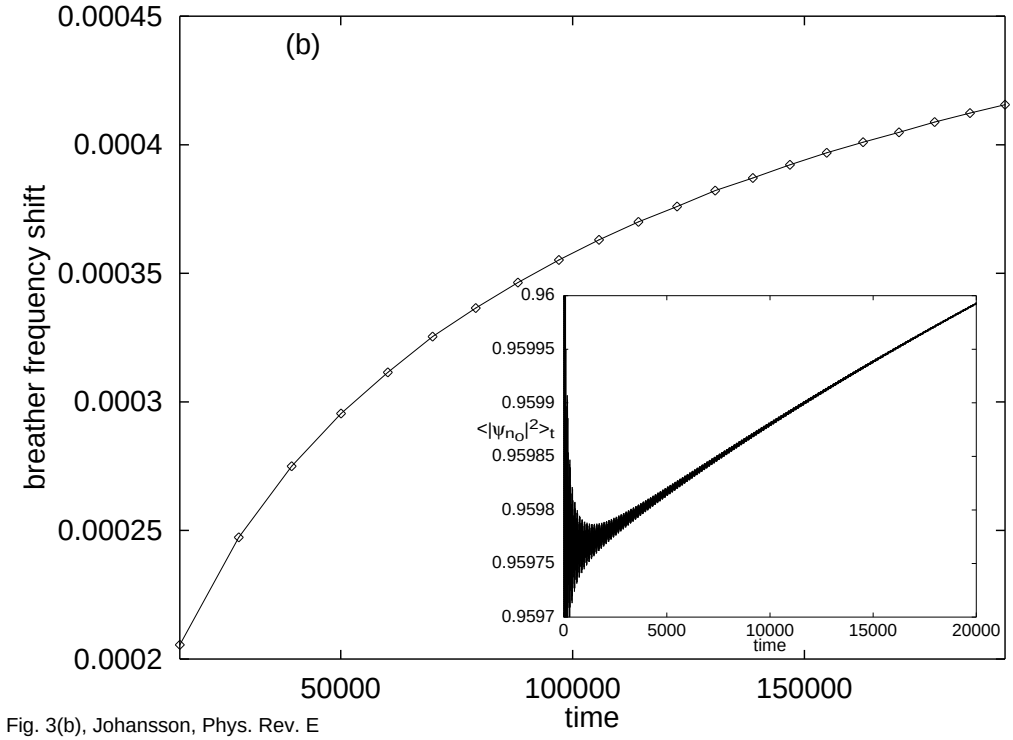

Fig. 3(b), Johansson, Phys. Rev. E

FIG. 3. Time-evolution of a breather with an initial perturbation in the direction of the pinning mode. Parameters are $\Lambda = 0.45$, $\omega_p \approx 0.197$, and $C = 1$. (a) shows the time-evolution of $|\psi_{n_0-1}|^2$, where n_0 is the central site of the breather, (b) (main figure) shows the instantaneous shift of breather frequency $\Lambda(t) - \Lambda_0$, and inset in (b) shows the time-average $\left\langle |\psi_{n_0}|^2 \right\rangle_t$.

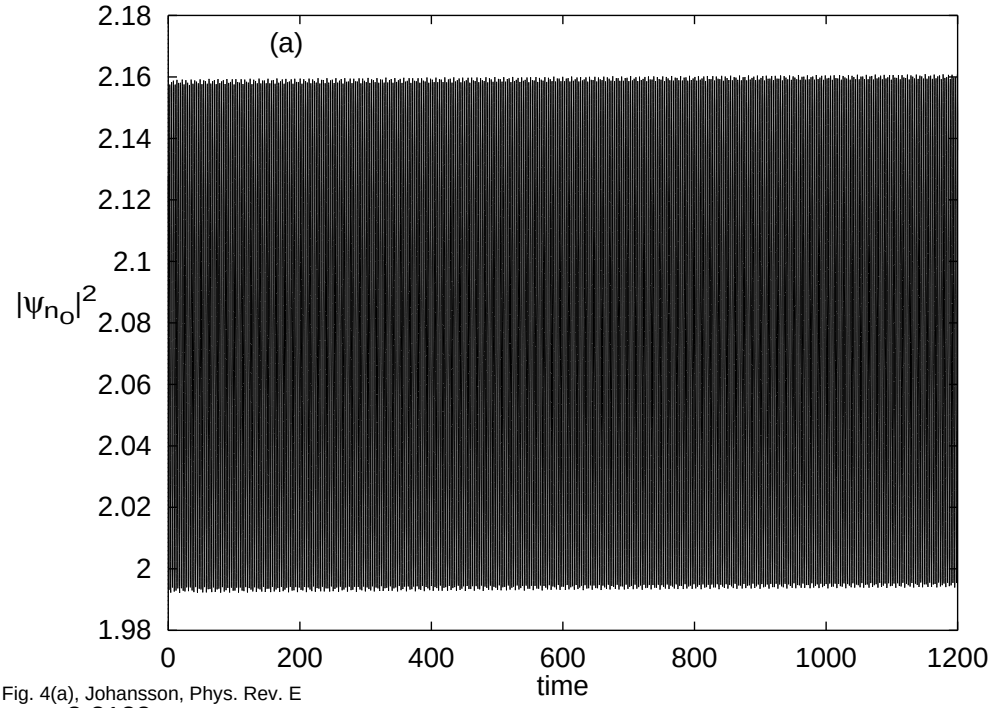

Fig. 4(a), Johansson, Phys. Rev. E

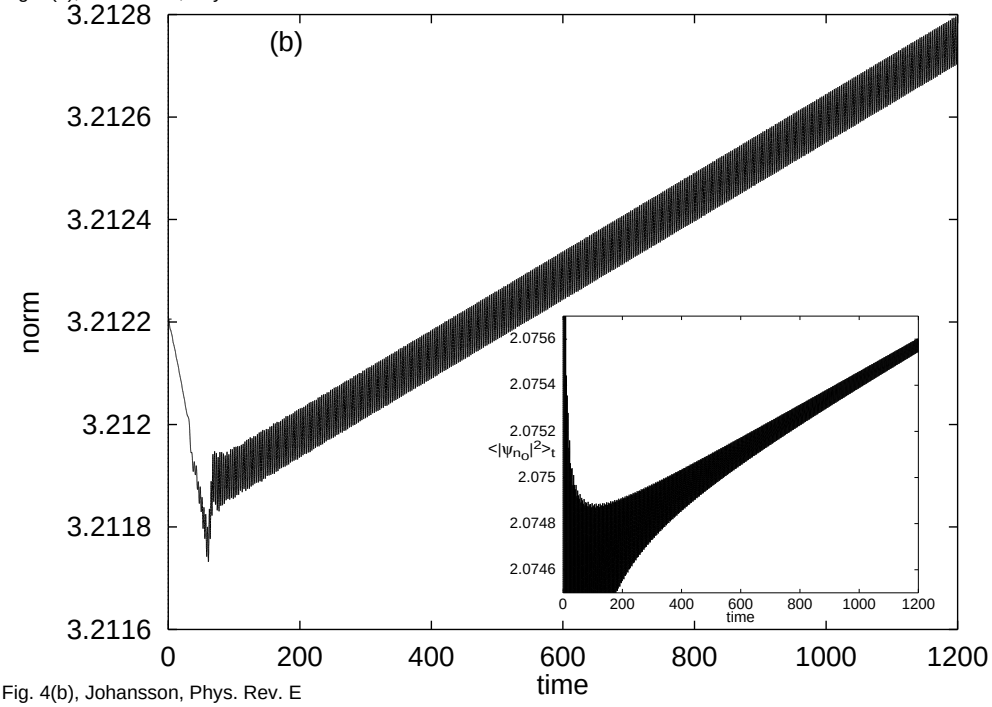

Fig. 4(b), Johansson, Phys. Rev. E

FIG. 4. Time-evolution of a breather with an initial perturbation in the direction of an extended eigenmode (spatially symmetric) with $q < q_c$. Parameters are $\Lambda = 1.0$, $\omega_p \approx 2.31$ ($q \approx 1.22$), $a \approx 0.0383$, and $C = 1$. (a) shows the time-evolution of the central-site intensity $|\psi_{n_0}|^2$, (b) (main figure) shows the total norm contained in a region of 120 sites around the breather, and inset in (b) shows the time-average $\left\langle |\psi_{n_0}|^2 \right\rangle_t$.

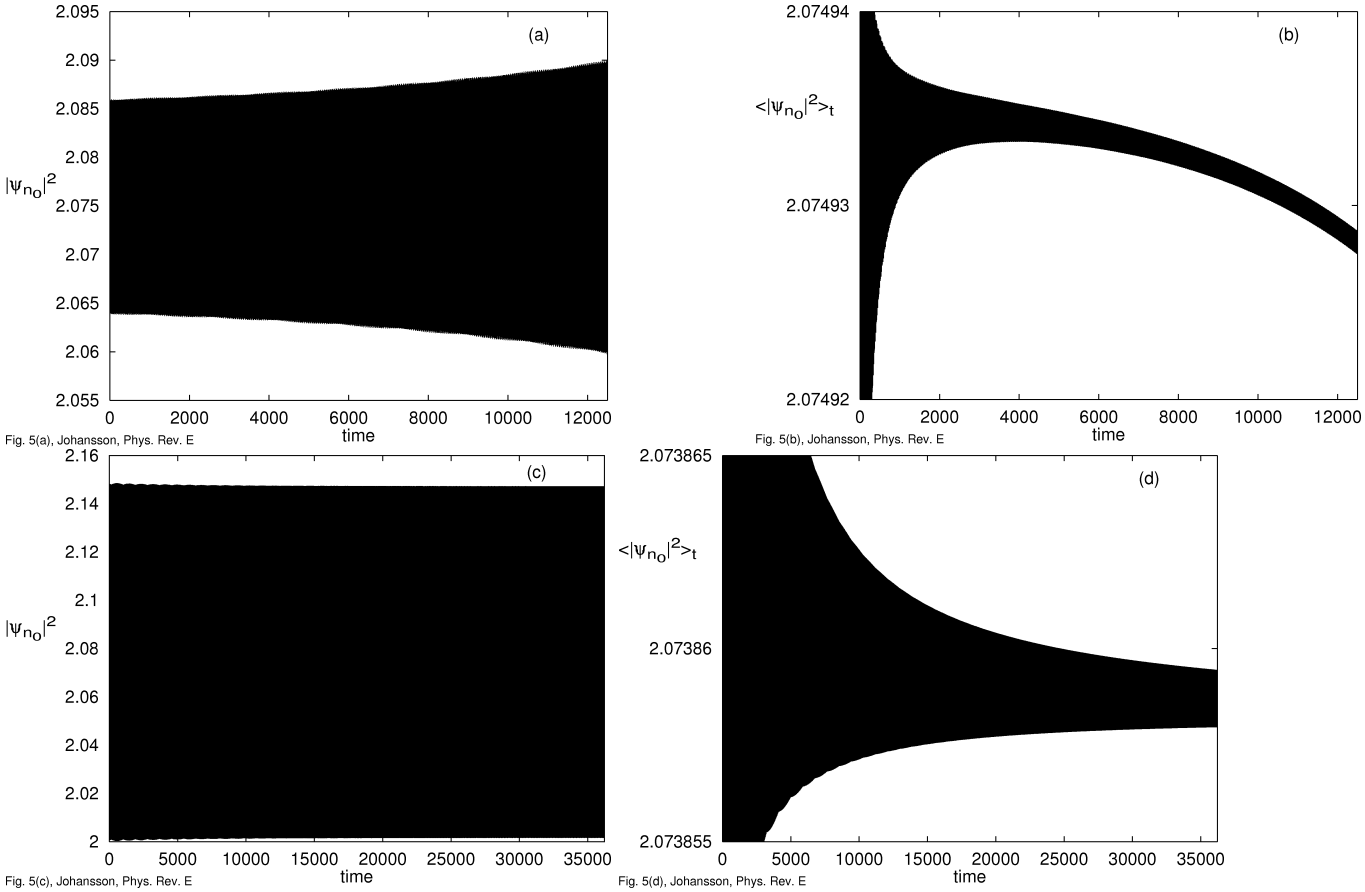

FIG. 5. Time-evolution of a breather with initial perturbations in the direction of extended eigenmodes with $q > q_c$. Parameters are $\Lambda = 1.0$, $C = 1$, and in (a), (b) $\omega_p \approx 4.93$ ($q \approx 2.88$) and $a \approx 0.0644$, resp. in (c), (d) $\omega_p \approx 2.72$ ($q \approx 1.43$) and $a \approx 0.0383$. (a), (c) show the time-evolution of the central-site intensity $|\psi_{n_0}|^2$, while (b), (d) show its time-average.

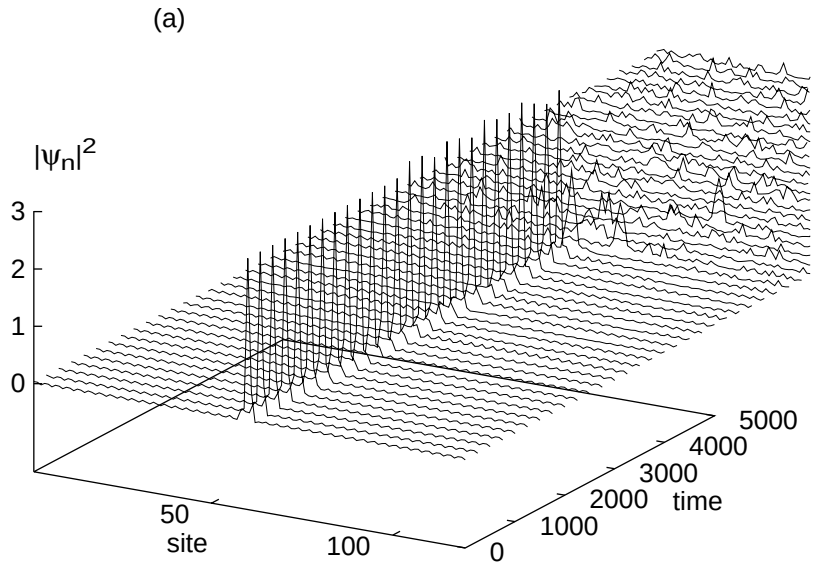

Fig. 6(a), Johansson, Phys. Rev. E

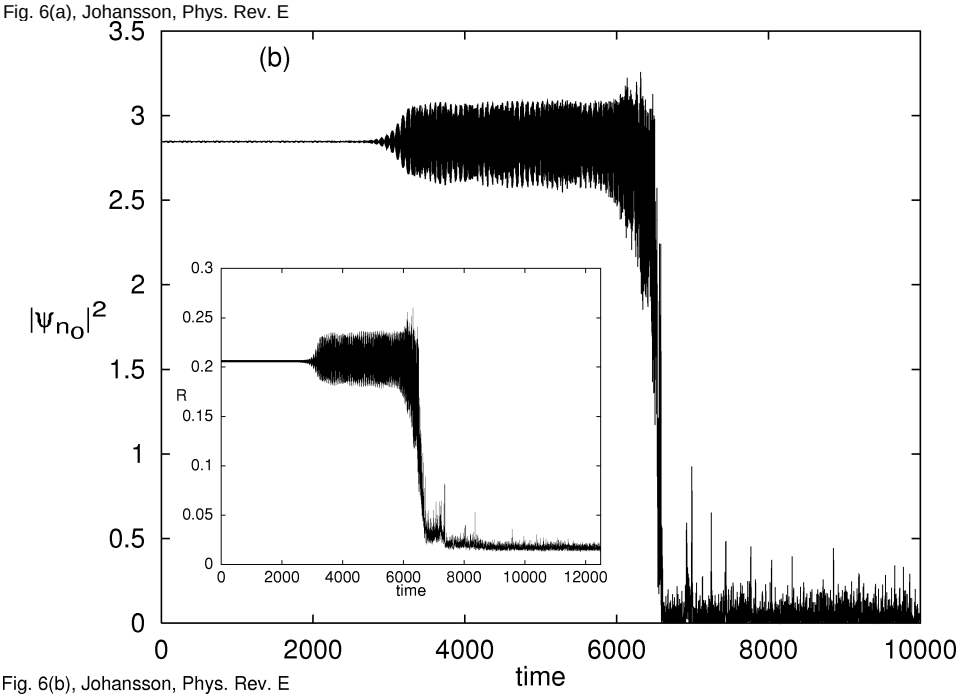

Fig. 6(b), Johansson, Phys. Rev. E

FIG. 6. Time-evolution of the phonobreather (56) with $q = 2\pi/3$ for a system of 120 sites (periodic boundary conditions), perturbed only by the numerical truncation errors. The breather frequency is $\Lambda_b = 1.55$, phonon frequency $\Lambda_{ph} = -2.95$ (phonon amplitude $a \approx 0.2$), and $C = 1$. (a) shows $|\psi_n(t)|^2$, while (b) (main figure) shows the intensity of the breather central site $|\psi_{n_0}|^2$. Inset in (b) shows the inverse participation number $R = \mathcal{N}^{-2} \sum_n |\psi_n|^4$, which gives a qualitative measure of the degree of localization.

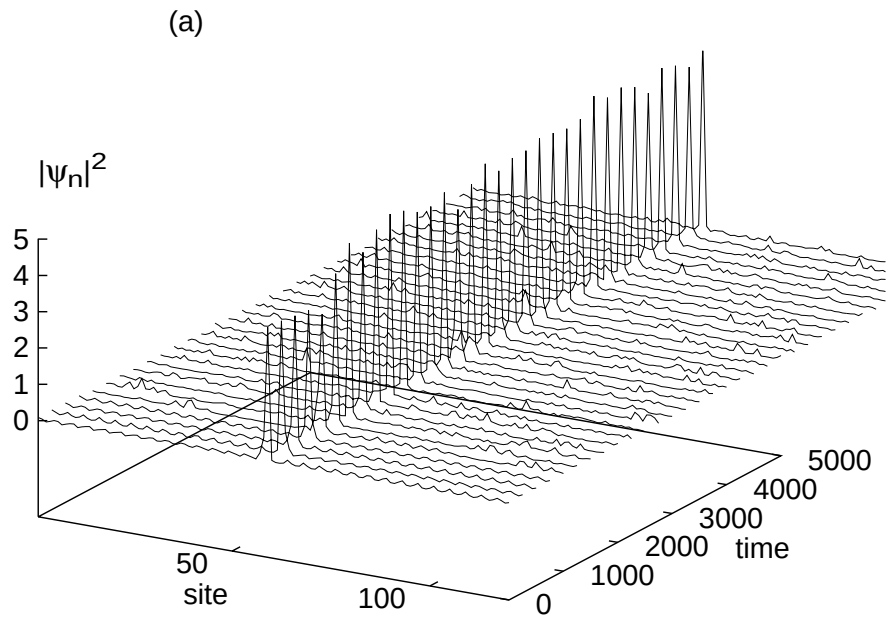

Fig. 7(a), Johansson, Phys. Rev. E

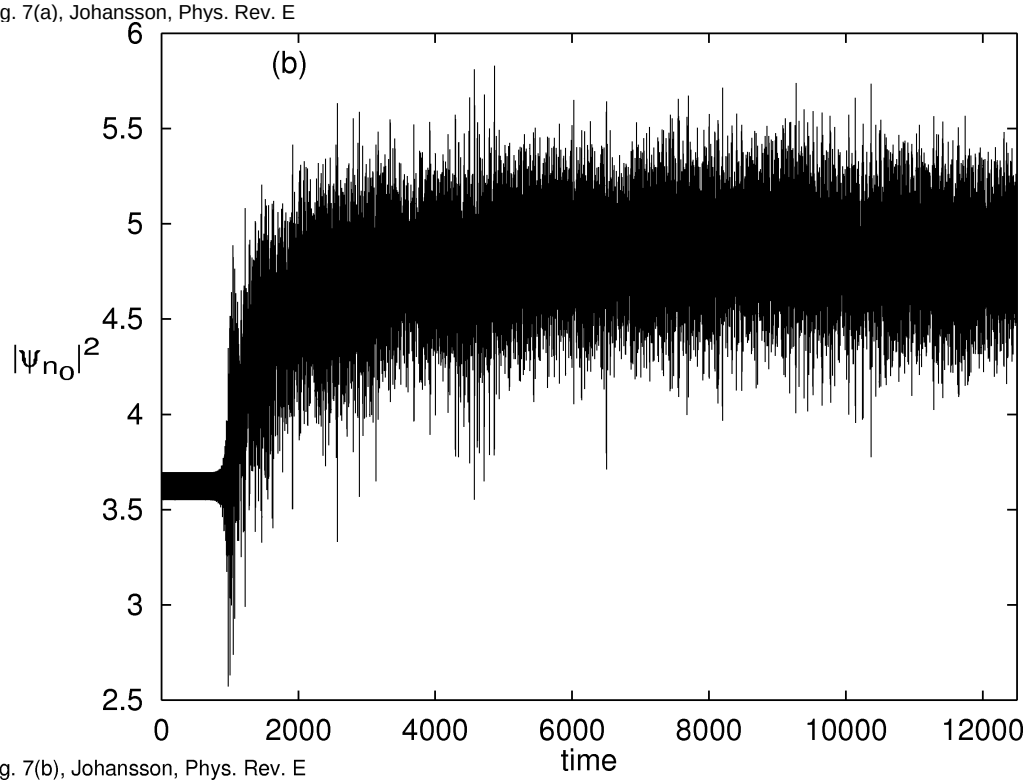

Fig. 7(b), Johansson, Phys. Rev. E

FIG. 7. Time-evolution of the phonobreather (58) with $q = \pi/4$ for a system of 120 sites (periodic boundary conditions), perturbed only by the numerical truncation errors. The breather frequency is $\Lambda_b = 2.2$, phonon frequency $\Lambda_{ph} = -0.5$ (phonon amplitude $a \approx 0.3$), and $C = 1$. (a) shows $|\psi_n(t)|^2$, while (b) shows the intensity of the breather central site $|\psi_{n_0}|^2$.